6. 1961-1990 high-resolution solar radiation climatologies for Italy

6.1 The role of the solar radiation in the Earth's energy budget

The solar energy is the primary energy source for Earth. It drives the atmospheric and oceanic circulations. In fact, the Sun provides 99.8% of the energy used for all natural processes (the rest is mainly geothermic energy, *Dickinson et al., 1980*) and approximately 1.779×10^{11} *MW* is the energy per second directly or indirectly used by the biosphere *(Iqbal, 1893)*. Furthermore, the solar radiation drives the Earth's climate and slight variations in the activity of the Sun (for example in the number of sunspots in the 11-year Sun cycle) may be responsible for global warming or global cooling. The seasonal cycle of the Earth is caused by the angle (23.5°) between the Earth's spin axis and the normal to its orbit. That is why, in the Northern Hemisphere, summer is much warmer than winter and the poles are colder than the tropics. The revolving orbit of the Earth around the Sun is an ellipse and it leads to a different energy budget between January and July (7% in favor of January, *Zaksek et al., 2005*).

The solar radiation travels through the universe without losing energy until it reaches the upper border of our atmosphere *(Brooks, 1952).* Then it experiences the various filtering and multi-scattering processes in the Earth's atmosphere; aerosols, water vapor, dust, smoke and clouds reduce the solar intensity that reaches the ground surface *(Coops et al., 2000)*.

The solar spectrum can be divided into short-wave and long-wave radiation; the short-wave is split up into direct, diffuse and reflected components and when a body (e.g., a cloud) absorbs shortwave solar radiation, it emits as long-wave solar radiation.

The global net radiation received by a surface rules many processes. These include the evapotranspiration, the sensible heat flux (i.e. the enthalpy) and the photosynthesis, the snowmelt, the plant life biological cycles, the macro-scale and the micro-scale processes as the air/soil heating, the turbulence layers mixing, winds, the hydrological

processes such as the water balance, and the energy budgets (particularly important for the architecture of buildings). In literature, it is easy to find many scientific applications of solar radiation models (e.g., *Dubayah 1994; Pinker et al., 1995; Varley et al., 1996; Gueymard, 2001; Wong et al., 2001*).

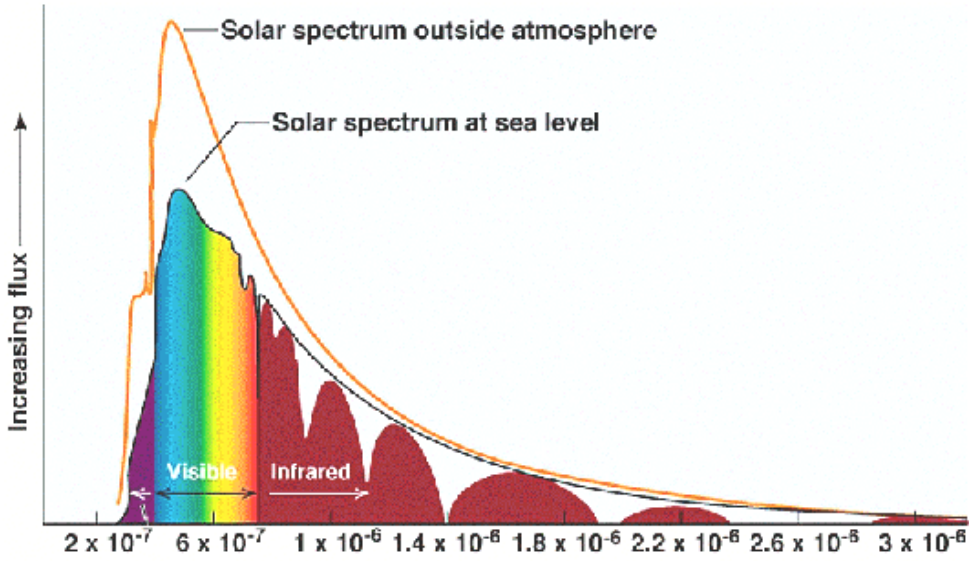

Fig. 158: The solar radiation spectrum outside atmosphere and at sea level (http://usr-lazio.artov.rm.cnr.it/concluse/scienza2001/modulo-snaturali/dimenno/irraggiamento.htm)

6.2 The global solar radiation components: direct, diffuse and reflected radiation

A complete solar model should evaluate the global radiation and its components, that are direct, diffuse and reflected radiation.

Direct radiation depends basically on the angle between sunrays and the normal to the ground surface (the solar angle of incidence), the solar declination angle, and the solar azimuth angle *(Pierce et al., 2005)*. It also depends on the transmissivity of the atmosphere, and on the optical depth of the atmosphere *(Coops et al., 2000, Muneer et al., 2000; Pons et al., 2008)*.

Diffuse radiation depends especially on turbidity (turbidity factor is often used as the Linke's factor), the sky view factor *(Pierce et al., 2005)*, and on the optical depth. It also depends on the wavelength of the sunbeams *(Coops et al., 2000)*, the cloud density and

type, elevation *(Kondratyev et al., 1970; Bitanja et al., 1996)* and on the unobstructed part of the overlying atmosphere (*Dubayah, 1994)*.

Reflected radiation is a shortwave radiation and depends on the obstructed part of the overlying atmosphere *(Dubayah et al., 1995)*, the terrain slopes, the foreground albedo and in most cases, in solar models. The reflected radiation is neglected *(Coops et al., 2000; Pons et al., 2008)*, even though it could be important in iced or snow-covered regions, as for very low Sun height angle (reflection by aerosols and other molecules because of the long optical path).

The direct component is by far the most important one in clear sky days, but in partly or totally cloudy days, the diffuse part is not negligible. Indeed in some cases, diffuse radiation is greater than direct radiation *(Coops et al., 2000)*. Generally, on clear sky days, the global radiation at the Earth's surface depends mainly on the direct radiation, and only 16% of the total radiation is diffuse in the visible solar spectrum between green and red *(Dubayah, 1992)*.

The diffuse component becomes increasingly important in mountain regions, because an area can be shaded by obstacles and mountains and may never receive direct radiation in winter months, depending on the Sun's inclination, on month, on slopes of the surroundings mountains and so on. It is very important to account for the topographic shading. This phenomenon, and the different insolation on slopes with different exposures, can lead to dramatic errors in an experimental solar model. *Wilson et al., (1970)* found differences up to 10 °C for north-facing surfaces versus south-facing surfaces in soil (a few centimeters below the surface) temperatures. *Dixon (1986)* found differences up to 12 °C for maximum temperatures for areas shaded by woods versus bare ground areas. In some cases a south-facing slope can receive up to three times the solar global radiation in winter in the Northern Hemisphere in contrast to a north-facing one (*Klein et al., 1977)*. For more details see *Fu et al. (2002)*.

In mountain regions, even the reflected radiation can play a role (especially in bare areas, over glaciers or snow-covered regions).

Thus, on clear days, the direct radiation dominates, especially in flat areas. The diffuse component depends only on the turbidity of the atmosphere, whereas in regions with a complex topography, the diffuse radiation plays a significant role. On cloudy days, cloudiness can reduce to 100% (usually the reduction is smaller than 30% for clear days, see *Gautam et al., (2002)*) the direct radiation, so it is fundamental to quantify not only the

direct radiation but also the diffuse radiation and the reflected radiation that reaches the ground.

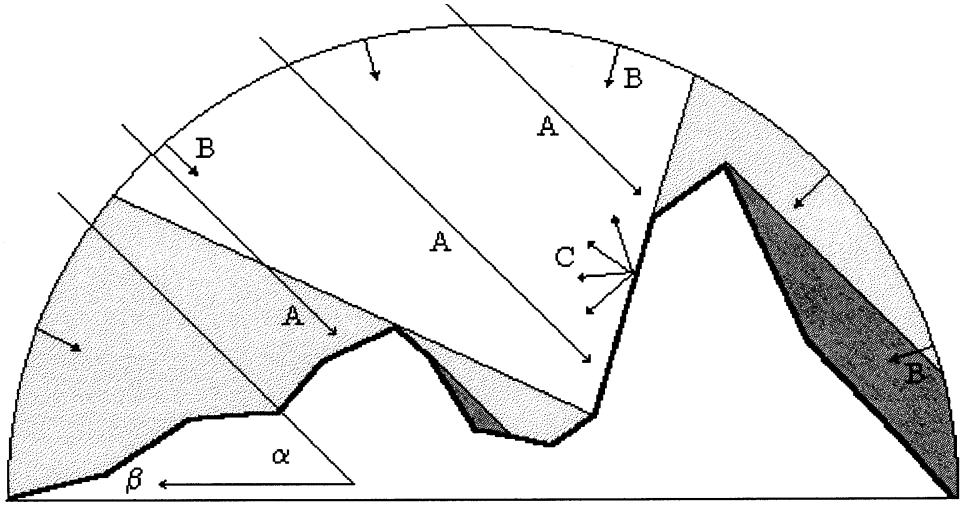

Fig. 159: The components of incoming solar irradiance: (A) direct irradiance; (B) diffuse sky irradiance; (C) irradiance reflected by nearby terrain (α is the solar elevation angle, β is the solar azimuth) (Antonic, 1998).

6.3 How to construct a solar model: different approaches

Let us briefly describe the most common approaches used in scientific literature to construct a solar radiation model. We divide them into main categories: models based on radiation measurements, and models based on theoretical calculations and approximations (subdivided into clear sky models and real atmosphere models).

6.3.1 Models based on radiation data from ground stations or satellites

If radiation data (global radiation data or single radiation component data) are available, a spatialization model can be used to obtain solar radiation gridded climatologies, see e.g. *Pons et al. (2008)*. The most used spatialization model for solar radiation is kriging, see Chapter 3. If only global radiation data are available, theoretical decomposition models that use global radiation to obtain diffuse and direct radiations can be used *(Gates, 1980)*.

Such radiation data can be obtained from station records (pyranometers or pyrheliometers for sunshine duration or radiation measurements, human observations for cloudiness, *Dubayah, 1992; Dubayah, 1994*) or satellite remote sensing data *(Gupta et al., 1999)*. Pyranometer records show a main problem: they are usually sparse and sited far from areas in total or partial shadow. Thus they can only be used to model the radiation for horizontal surfaces. On the other hand, there is a general skepticism about satellite data for climate studies because of their low degree of reliability, aside from the fact that it is hardly possible to create high-resolution models using only satellite records. In fact, they are frequently used to get low-resolution maps only *(Petrarca et al., 2000*; *HELIOSAT* model, *Cano et al., 1986*).

The main difference in quality between solar radiation models is caused by the availability of meteorological values and weather information; *Zaksek et al., (2005)*, for example, evaluating the importance of the various proxies that can be used for a solar radiation model. The slope and facet parameters are extremely important, the meteorological data are very important, the quality of the *DEM* is quite important, and the astronomical parameters can be roughly approximated in a physical model for quasi-global radiation.

6.3.2 When radiation data are not available: clear sky solar models

When no measured radiation data are available, as in the most cases, the solar radiation models are based on theoretical calculations only and can be distinguished between clear sky models and a real atmosphere model.

We define "clear sky" as a completely cloudless sky in a clear atmosphere that does not filter or scatter solar radiation. If the atmosphere is non-interacting, the global solar radiation received by a surface on the Earth is exactly the same that a surface on the upper limit of the atmosphere with the same inclination receives (the so-called exo-atmospheric radiation), because no attenuation occurs.

This type of model is based on geometric and astronomic parameters for the Sun's position to the Earth's Surface at any time of the year for any geographical coordinates, on complex calculations related to the topographical shading that the real Earth's rugged terrain causes. Some authors use pre-packed *GIS* tools for calculations about shading, such

as *OMBRA, INSOLDIA* (*Pons et al., 2008*), *HILLSHADE, MOD-SHADOWS (Kumar et al., 1997)*.

By means of mathematical formulas and approximations, clear sky models provide direct radiation and reflected radiation values for every grid point of a *DEM* for every month or day. They provide radiation values for flat surfaces or sloped surfaces and they include encoded tools that account for shadowing parameters.

Such models cannot be used as information for other climatic variables that describes real atmosphere conditions, but they are used in engineering, especially for photovoltaic energy applications *(Suri et al., 2004)*.

6.3.3 When radiation data are not available: real atmosphere solar models

The solar radiation is filtered by the atmosphere before reaching the Earth's surface; the atmosphere scatters the radiation (air molecules, aerosols, pollutants), absorbs the radiation (ozone, water vapor, oxygen, carbon dioxide and so on) or both processes can occur simultaneously (in clouds, for example, *Jacovides (1997)*). In real atmosphere conditions, the solar radiation is split up into direct and diffuse radiation. They both contribute to the reflected component, where the ground albedo is high and the sky view is obstructed by surrounding surfaces.

Because of the scattering properties of the atmospheric molecules, the diffuse radiation is usually considered as isotropic and not changing during the day in solar radiation models *(Kondratyev et al., 1970*; *Antonic, 1998; Chung et al., 2004a)*. However, this is an approximation (a very good approximation for a solar radiation model), because, actually, the diffuse radiation is anisotropic *(Allen et al., 2006)*.

The solar radiation models for real atmosphere also deal with astronomical quantities and orographic parameters such as solar radiation models for clear sky conditions.

When no radiation data are available, we can divide solar radiation models for real atmosphere into: parametric models that need atmospheric quantities from data *(Dubayah, 1992; Gueymard, 2001)*, models based on sunshine duration or cloudiness data (70-85% of variance related to insolation can be explained studying sunshine duration; 50% of variance using cloudiness, see *Bennett, (1969)*), solar spectral irradiance models *(Gueymard,*

2001), and downloadable ready to use GIS solar models (even though they are rarely implemented with real atmosphere features).

All the listed models provide final global radiation results by means of empirical formulas, theoretical considerations, approximations and gridding techniques (*Angstrom, 1924; Muneer, 1999; Page et al., 2001)*.

• Parametric models

Parametric models model the global solar radiation and its components starting from a scattering-absorption point of view. This approach requires a detailed description of the atmospheric layers and composition. The principal disadvantage lies in the need of a great number of physical and chemical parameters that are rarely available or that are available only at a local-scale.

Such models can be divided into two categories: the first deals with the filtering properties of the single atmospheric components and these models threat direct and diffuse radiation separately *(Pinker et al., 1985; Wong et al., 2001; Wang et al., 2006a)*, and the latter deals with a special turbidity factor (Linke's factor or Angstrom's coefficient), with the optical air mass and with pressure corrections with elevation (*Jacovides, 1997; Rigollier et al., 2000)*. Some authors use simpler model based only on the optical air mass and on the water vapor absorption of the radiation (e.g., *Revfeim, 1997*).

In parametric models which deal with the filtering properties of the single atmospheric components, the atmospheric attenuation of the direct solar radiation is usually evaluated using the Lambert Beer's equation (see next paragraphs for details). In such models, the diffuse component is evaluated by taking into account the Rayleigh's scattering after the first passage of the radiation through the atmosphere, the aerosol scattering after the first passage of the radiation through the atmosphere, the multiple reflection and scattering processes between the sky and the ground. For a horizontal surface, the Rayleigh and the aerosol scatterings for the diffuse radiation depend on the solar zenith angle, the transmittance parameters, and on a "forward scattering" function. The multiple scattering depends on the solar elevation, the ground albedo and on the cloudless sky albedo (*Wong et al., 2001, Ranzi et al., 1995)*.

The second type of parametric models describe the atmospheric transmittance using two special coefficients: the Linke's turbidity factor (indicated with T_L; *Linke, 1922*) and the

Angstrom's coefficient (indicated with β; *Angstrom, 1964*); they correct the optical air mass for elevation, refraction of the solar radiation and for pressure *(Kasten et al., 1989)*.

The Linke's factor depends especially on air mass, water vapor, gases and aerosol *(Rigollier et al., 2000)* and represents the number of clean dry atmosphere necessary to produce the same attenuation of the real atmosphere. The average value for Europe is 3.5, but it varies locally. The attenuation increases with T_L because a higher turbidity means a higher scattering and absorption processes. T_L depends on the air mass (indicated with m) that is not available everywhere, hence this problem is often moved around imposing a constant value of $m = 2$ for calculating T_L *(Kasten et al., 1989)* or it is derived inversely from beam pyrheliometric measurements (*Jacovides, 1997*) and local data (*Kasten et al., 1984)*. The Linke's factor is the ratio between total optical depth and Rayleigh's optical depth: $T_L = 0$ means a non-attenuating atmosphere, $T_L = 1$ means a pure Rayleigh's atmosphere with no aerosols and only molecular scattering, $T_L = 3\text{-}4$ means a quite turbid atmosphere, $T_L = 6$ means a very dirty and polluted atmosphere.

The Angstrom's coefficient quantifies the scattering effects of the aerosols and it varies from 0 (very clear atmosphere) to 0.4 (very dirty atmosphere) (*Jacovides, 1997)*.

The combined used of the Linke's factor and the Angstrom's coefficient accounts for the attenuation of direct and diffuse radiation in a real atmosphere and for the diffraction and refraction effects *(Page et al., 2001)*. The Linke's turbidity factor is also used in *GIS* tools as *r.sun* and in the European Solar Radiation Atlas (*ESRA: Beyer et al., 1997; Rigollier et al., 2000; Page et al., 2001)*.

The Angstrom's coefficient is rarely used as an independent quantity in literature *(Jacovides, 1997*), but it is used to obtain a Linke's turbidity modified factor that accounts best for the aerosols and depends even on the Angstrom's coefficient *(Valko, 1961)*. Other authors (e.g., *Jacovides, 1997)* calculate the Angstrom's coefficient from Linke's factor obtained from pyrheliometric measurements and divide the atmosphere in rather dry, medium humid and very wet conditions, depending on the water vapor content.

• Spectral solar irradiance models

Spectral solar irradiance models are widespread in literature and are applied in climate studies, in engineering projects, in biology and so on *(Nann et al., 1992)*; these models can be made of sophisticated rigorous codes (*LOWTRAN, MODTRAN: Anderson et al., 1995)* or approximated transmittance parametric formulas. In the first case, the

atmosphere is considered as a set of vertical layers. In the second case the atmosphere is described with a set of parameters related to the single components (*SPECTRAL2: Leckner et al., 1978; Bird et al., 1984; Nann et al, 1992).*

• Decomposition models: from sunshine duration to radiation values

A very dense dataset of direct and diffuse radiation measurements (by pyranometers) is available in some regions only (i.e. East Anglia). On the other side, there is a high number of sunshine duration records worldwide and these records are spatially denser and temporally longer than the solar radiation series (*Revfeim, 1997).*

The basic idea is to correlate the so-called Clearness Index with the fraction of the solar radiation received by the surface in terms of the so-called Sun Hours Ratio *(Angstrom, 1924)*. The Clearness Index (usually indicated with K_t) is the ratio between the global radiation really received by a surface and the hypothetical global radiation received by the same surface on a clear sky day. To be precise, a slightly different one substitutes this definition, where the hypothetical global radiation is substituted by the exo-atmospheric value (i.e. the solar radiation at the upper limit of the atmosphere, *Martínez-Lozano et al., 1984*). Thus it considers the atmosphere as optical transparent to solar radiation on "perfect clear sky days". The Sun Hours Ratio is the ratio between the number of hours of sunlight received and the maximum number of hours of sunlight receivable (that is, from sunrise to sunset, varying for each day of the year) by a horizontal surface. It is often indicated with R_s or with S/S_0 (*Gueymard, 2001;* see next paragraphs for details).

The Angstrom's formula (see the next paragraphs) and its variants *(Angstrom, 1924; Martínez-Lozano et al., 1984)* permits to calculate the Clearness Index from the Sun Hours Ratio with a linear regression model. Consequently, from sunshine duration records, global radiation can be obtained.

In literature, many empirically improved calculations of K_t from R_s can be found. *Rietveld (1978)* and *Akinoglu et al. (1990)* used polynomial regression models. *Ampratwum (1999)* used a logarithmic model. *Revfeim (1981)* included atmospheric transmissivity parameters in the formula. *McArthur et al. (1981)* defined site-independent coefficients in the *LR*. *Iqbal (1983)* used also latitude as a independent variable other than R_s. *Gopinathan (1995)* used also latitude and altitude as independent variables, and other authors used also daily temperature range as independent variable and so on.

Furthermore, *Suhercke (2000)* revised the Angstrom's formula and introduced some considerations that theoretically hypothesize a non-linear correlation between the clearness index and the Sun Hours Ratio.

Some authors reviewed the various models on the Angstrom's formula. The accepted idea is that every model could be valid; the choice strictly depends on the geographical area of interest *(Ampratwum, 1999)*. Decomposition models are site-dependent models and the coefficients of the regressions are usually valid only for those single regions specifically studied, but some special cases hold good worldwide *(Gopinathan, 1995; Roderick, 1999)*.

Hypothetically, the diffuse fraction should increase as the clearness index decreases, because on an overcast day, the clouds play a leading role for the diffuse radiation. The diffuse fraction depends on the optical properties of the atmosphere, on volcanic eruptions *(Garrison, 1995)*, on global transport of dust or sand *(Moulin et al., 1997)*, but clouds dominate and in particular the cloud thickness, the cloud height and the cloud type (*Roderick, 1999*). The surface albedo could be neglected because it influences the reflected part of solar radiation more. The Northern Hemisphere has a higher diffuse fraction than the Southern Hemisphere because of the higher portion of emerged lands and the higher population density and industrialization that cause a higher aerosol and pollutants concentrations (enhancing the scattering of the solar radiation, *Roderick (1999)*).

Decomposition models are able to quantify the diffuse radiation component without diffuse radiation data *(Iqbal, 1983;Spitters et al., 1986)*. In decomposition models, the diffuse fraction of the global radiation received by a surface (or the diffuse index) is indicated with K_d or K_{dif} and it is usually obtained as a function of the Clearness Index *(Gopinathan, 1995)*. See the next paragraphs for details.

Some authors obtain the diffuse fraction by means of thresholds models. Depending on the Clearness Index value, they use different functions (based on the Clearness Index itself) to derive the diffuse fraction of radiation. This is the case in *Rodderick (1999)* for Australia, in *Jin et al. (2004)* for China, in *Orgill et al. (1977), Erbs et al. (1982), Olyphant (1984), Reindtl et al. (1990)* for USA and Canada, for Norway by *Olseth et al. (1986)* and so on.

In a review paper, *Wong et al. (2001*) states that each model can be suitable or not suitable, depending on the data availability, the time-scale frequency of data (a longer period is preferred because the weather conditions are averaged, so the statistical fluctuations in the results are less important), the geographical region and the weather

conditions. The Gopinathan's model is often pointed out as the most reliable one and, as we can see in the next paragraphs, we applied it in our solar radiation model for Italy.

A different decomposition approach derives the diffuse fraction from cloudiness data *(Kasten et al., 1980; Muneer et al., 1997; Muneer et al., 2000)*, but this could be dangerous because the cloudiness data are "measured" according to human-eye observations. That means a deep subjectivity of the cloud cover interprets in a yes-no binary system. These data are usually in okta (number of overcast parts in the sky divided into eight sections) but they can also be found in tenths.

In our opinion, it would be preferable to use cloudiness data only as a posteriori comparison of the diffuse fraction results, if sunshine duration data are available for the same stations. Cloud cover can only explain 50% of the solar radiation variance, whilst sunshine duration can explain the variance of the solar radiation up to 85% *(Bennett, 1969)*.

Once the diffuse and the direct components are derived, the reflected and the global radiation can be easily inferred (see the next paragraphs).

6.3.4 Solar radiation models as *GIS* models ready-to-use

Ready to use *GIS* (*GIS* means Geographic Information System) tools are mostly implemented in the *GRASS GIS* software (*http://grass.itc.it/*). Geostatistical models have advantages and disadvantages. On one side, they are ready to be downloaded, they are based on codes that calculate astronomical, geographical, shading parameters and in some cases they are connected with database that are daily or monthly updated. On the other side, they are usually not free, they use rough approximations in order to shorten the time to get results, they are sometimes adapted or converted form meteorological models, they are low-resolution models and the topography is rarely accounted for with a high degree of precision.

Here we only cite some examples: Solar Analyst 1.0 (Arcview ™ software, *http://www.esri.com/software/arcview/index.html*), Solar Flux *(Fu et al., 2000), r.sun* (*ArcGIS* tool used for the European Solar Radiation Solar Atlas, *ESRA*; *Suri et al., 2004*) and so on. Such models are conceptually similar; they mainly differ in the different geometric approximations used to evaluate the topographic shading. These models all produce rasters of direct and

diffuse (reflected is often neglected because the surface albedo at local scale is rarely available because of the lack of albedo grids) radiation without using real datasets, but a priori theoretical calculations only, thus they let the validation to the users. In literature, many authors do not rely on using this ready to use *GIS* models (e.g., *Zaksek et al. (2005)*).

The majority of these packages are implemented as clear sky models but in some cases they rely on real atmosphere conditions. The most detailed *GIS* tool on solar radiation is probably the *PVGIS* (Photovoltaic *GIS*, *http://sunbird.jrc.it/pvgis/*) created by *JRC* (Joint Research Centre of the European Commission, *http://ec.europa.eu/dgs/jrc/index.cfm*). It uses the Linke's factor, *WDRC* (World Radiation Data Center of *WMO*, World Meteorological Organization, *http://wrdc.mgo.rssi.ru/*) station, satellite global radiation data, astronomic quantities, high-resolution topography and shading calculations (by *M.Suri* and *T.Hudd*, *http://sunbird.jrc.it/pvgis/solrad/index.htm*).

6.3.5 Other methods used to obtain a solar radiation model

• Inverse model: from temperature data to global radiation

If no radiation data are available, but mean monthly minimum and maximum temperatures are at disposal, such data can be used to derive solar radiation components (this method should not be applied for daily calculations, *(Erbs et al., 1982)*). These inverse models *(Coops et al., 2000)* start from temperature extremes in order to obtain the atmospheric transmissivity.

Bristow et al., (1994) used this technique and they performed a validation with a small set of diffuse and direct measurements. The model works satisfactorily for flat surfaces (error lower than 1%). However, it does not perform well for inclined slopes (the mean absolute error is approximately 10% and increases with increasing inclination of slopes, probably because in this case the reflected shortwave radiation, not considered in this model, plays a non-negligible role).

- **The *ASHRAE* model**

The *ASHRAE* model *(ASHRAE book, 1977)* is a solar model widely used in engineering studies and in climate papers *(Wong et al., 2001)*.

This model is based on the atmospheric attenuation properties, on the Clearness Index and on the real pressure correction for optical depth of the atmosphere, but the Earth curvature is not considered in the calculations. A simplified version of this model neglects the reflected radiation in areas where the ground albedo is unknown. See *ASHRAE (1977)* for details.

- **The Varley's model**

The Varley's model is a hybrid model based on the optical properties of the atmosphere and the Clearness Index *(Varley et al., 1996)*. The transmission factor of the atmosphere is used as a function of the Clearness Index itself by means of empirical local coefficients. Thus this approach cannot be reproduced globally. This is the opposite limitation that most solar radiation models are not able to overcome, i.e. the non reproducibility of global-scale solar models to small areas *(Antonic, 1998)*.

6.4 1961-1990 high resolution solar radiation model for Italy

6.4.1 Motivations and methodology

We supposed that the final statistical errors of our temperature model for 1961-1990 for Italy would improve if we model the global solar radiation received by every single grid cell (using the *USGS GTOPO30* digital elevation model) and if we use this quantity as an independent variable. Temperature is supposed to be correlated with solar radiation, especially with global radiation, and it is well known that climate models would benefit from radiation budget parameterization, for example, 5% for a 1,000-km monthly scale *(Leith, 1973)* and much more for a 1 km^2 monthly scale. At last, many authors have already created solar radiation models in order to use solar radiation as a variable for other models

(e.g., *Ninyerola et al., 2000; Fu et al., 2002)* and in many cases they obtained a great improvement.

Thus, we decided to create a solar radiation model for Italy, i.e. a mathematical model that is based on measured data, which uses astronomical parameters, considers the effects of topography and is able to define a global radiation value for each grid cell. Such a model accounts for spatial (topography and geographical variables as latitude and longitude) and temporal variations (the Sun's position at every hour, day, month of the year) as suggested by *Dozier (1981)*.

Our idea was to combine sunshine duration and cloudiness quality-checked data with topographical high-resolution calculations, in order to get the first high-resolution solar radiation model based on station data for Italy.

First, we collected 1961-1990 sunshine duration data, we quality checked and used them in order to calculate the Clearness Index and the diffuse fraction values that led us to obtain monthly diffuse radiation and direct radiation received by a flat surface. Second, from the direct radiation component, we empirically evaluated the turbidity Linke's factor and we created low-resolution 1961-1990 turbidity maps for Italy. Third, we wrote algorithms based on astronomical parameters and orographic parameters (i.e. the shading factors) in order to calculate diffuse and direct radiation components for sloped surfaces using the *USGS GTOPO30 DEM*. Fourth, we derived albedo raster grids from *GLC2000* land cover maps and from tabled albedo parameters and we used them to calculate reflected radiation component for each grid cell. Fifth, we summed up direct, diffuse and reflected radiations in order to obtain hi-res global solar radiation grids for Italy related to 1961-1990 period. Sixth, we used the albedo values to get absorbed radiation grids.

The lack of solar radiation models for Italy (the only available solar models for Italy are *GIS* models as *r.sun* by *Suri et al. (2004)* which have a low spatial resolution, or satellite-derived maps of solar radiation as by *Petrarca et al. (2000),* or very low resolution models for global and diffuse radiation by *Lavagnini et al. (1990), Lavagnini et al. (1991)*) convinced us to refine the methodology as to obtain a solar radiation model that can be even adjusted for energetic and photovoltaic applications. In the end, we used such global radiation grids in temperature climatologies (see Chapter 4).

As we can see in the next paragraphs, we used a quality checked but not homogenized 1961-1990 sunshine duration dataset. In the future, we plan on realising a

solar radiation model that will be based on a homogenized larger dataset, which includes station data from different time intervals opportunely converted to 1961-1990 by means of gridded anomalies.

Other developments will be the construction of solar radiation models based on cloudiness data or global radiation data. Such models could be used as a validation test for our model based on sunshine duration data (eventually homogenized).

6.4.2 Data search: global radiation, cloudiness and sunshine duration data

• Global radiation data

First, we searched for global radiation data, but we found no time series but 33 monthly normals on the website of the Aeronautica Militare Italiana (*http://clima.meteoam.it/*), 2 monthly normals on the 1966-1975 *ESRA Vol. 1* (European Solar Radiation Atlas, *Kasten et al., 1984*) and no time series. We also found, in the *DBT-ENEA* database (*http://clisun. casaccia.enea.it/*), 738 1994-1998 monthly normals, but these data were derived from satellite observations and we did not accept satellite data.

Out of the 35 station data normals, only 24 have 30 years of data in our 1961-1990 reference period, thus we concluded that this dataset was not suitable to implement high-resolution solar radiation grids.

• Cloudiness data

Second, we searched for cloudiness data and we obtained: 47 series from Air Force (35 of these cloudiness series were homogenized and used in *Maugeri et al. (2001)*), 148 monthly normals in the *DBT ENEA* database (*Petrarca et al., 1999)* and 29 normals from the *SCIA-APAT* website (*http://www.scia.sinanet.apat.it/*) labeled as *UGM-ENAV* (Ente Nazionale di Assistenza al Volo).

153 out of these 224 records are related to our 1961-1990 reference period and the others could be converted into 1961-1990 normals by means of cloudiness anomalies grids in *Maugeri et al., (2001)*. Nevertheless we decided to use sunshine duration data instead of

cloudiness data because the latter ones are more subjected to human errors and because sunshine duration records are usually better correlated with solar radiation than cloudiness (see Chapter 6.3).

• Sunshine duration data

As **time series** we found:
- monthly series from the *SCIA-APAT* dataset (*http://www.scia.sinanet.apat.it/*) subdivided into: 121 from *UCEA*, 49 from *ENAV* (Ente Nazionale di Assistenza al Volo), 51 from regional *ARPA*s (especially for Friuli Venezia Giulia and Marche): 221 stations;
- monthly series from the European Solar Radiation Atlas (vol. 1, *Kasten et al., 1984)*: 2 stations;
- daily series from *MIPAF* (Ministero delle Politiche Agricole e Forestali, *http://www.politicheagricole.it/default.html*): 39 stations.

As **monthly normals** we found:
- monthly normals from Meteo France (*http://france.meteofrance.com/*): 5 stations;
- monthly normals from Meteo Swiss (*http://www.meteoswiss.admin.ch/web/en/weather.html*): 15 stations;
- monthly normals from *ARSO* (Agencijea Republike Slovenije za okolje (*http://www.arso.gov.si/*): 1 station;
- monthly normals from monographic books (Vercelli: *Cat Berro et al., 2005*; Aosta: *Cat Berro et al., 2003*): 2 stations;
- monthly normals from *ZAMG* (*http://www.zamg.ac.at/*): 7 stations;

We collected a database of 292 sunshine duration records for the Italian region and its surroundings. After a first quality check on geographic position, elevation and duplicated stations, we obtained a database of 236 stations.

A second quality check procedure was based on data and we accepted:
- records with at least 20 years of data in 1961-1990 period:
  - a year was considered valid only if all monthly data were available;
  - a month was considered valid only if a record had more than 25 daily data (23 for February).

In case of two or more stations located very close with the same name, we chose the stations with the highest number of valid years in 1961-1990 period and fully-reported metadata.

After this second check, our 1961-1990 sunshine duration dataset was made of 54 stations. Let us show the 1961-1990 sunshine duration dataset distribution for Italy.

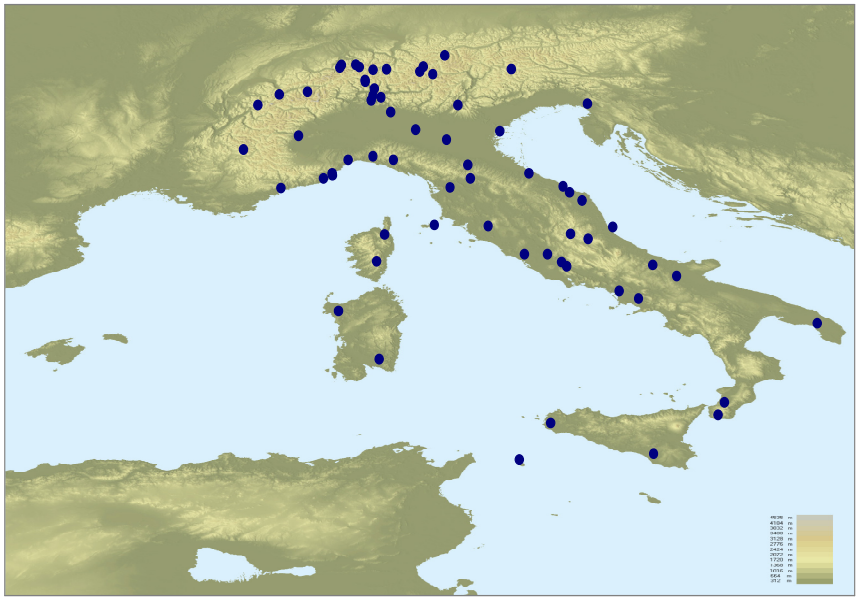

Fig. 160: Sunshine radiation 1961-90 station distribution for Italy

From fig. 160, it can be seen that such a station distribution is not dense enough to represent the average 1961-1990 spatial distribution for sunshine duration in Italy. Even if the 30-year average condition of the atmosphere (i.e. clouds, fog, pollution and so on) can be described with a lower resolution than precipitation or temperature.

We decided to expand our dataset by including data not related to 1961-1990, but some introducing commentaries are necessary. We could not expand our 1961-1990 sunshine duration dataset by converting our dataset to 1961-1990 with a gridded anomaly approach as for temperature and precipitation datasets. This is because we did not have a secular homogenized sunshine duration database as Spain does *(Sanchez-Lorenzo et al., 2007)* which can be used to create monthly anomaly grids. Unfortunately, the longest complete series are relative to 1956-1996 period and only 4 series are relative to 1951-2006, thus it was not possible to create anomaly grids for time series of sunshine duration.

It is well demonstrated that sunshine duration, as solar radiation, is not constant through decades. Solar radiation secular records show a "global early brightening" period

approximately between 1940 and 1950, a "global dimming" period approximately between 1950 and 1980 and a "global late brightening" period approximately after 1980 *(De Bruin et al., 1995; Gilgen et al., 1998; Wild et al., 2005; Ohmura, 2006; Sanchez-Lorenzo et al., 2007; Wild, 2009)*.

In the following picture we show the global radiation trend for Stockholm, where the brightening and dimming periods can be easily recognized.

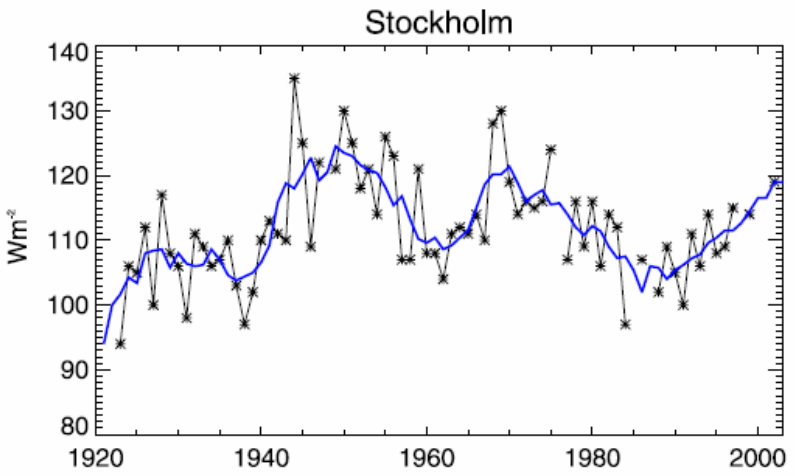

Fig. 161: Solar radiation time series of Stockholm: brightening and are evident (Wild, 2009)

Furthermore, solar radiation and sunshine duration are subjected to great volcanic explosions such as El Chicon (Mexico, *Heimo et al., 1989*) in 1982, Pinatubo (Philippines, *Molineaux et al., 1996*) in 1991, and Mount Redoubt (Alaska, USA) in 1966. Thus sunshine duration data not related to our 30-year reference period should be handled with care.

In the following picture we show the solar radiation transmission from the Mauna Loa observatory. The volcanic eruptions and explosions greatly reduce the solar transmission and, moreover, they usually cool the global temperature.

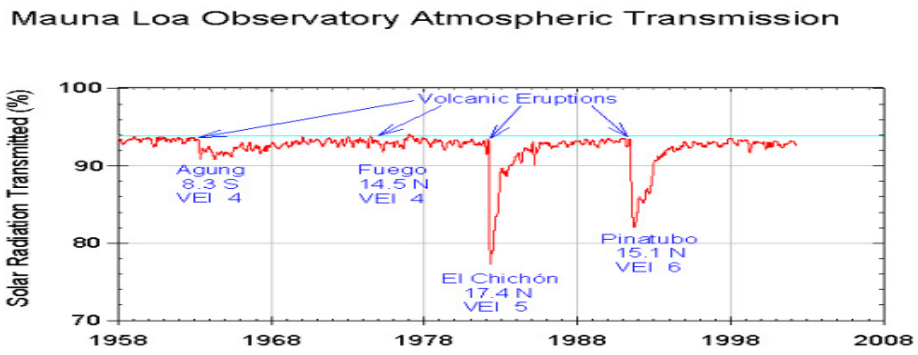

Fig. 162: Solar Radiation Transmission in % from Mauna Loa Observatory: after two massive volcanic eruptions, El Chicon and Pinatubo, solar radiation transmission dramatically decreased (NOAA website)

We decided to expand the Italian sunshine duration dataset used in this work by including every station with at least 10 valid years in the 1951-2007 period. Then we cross-checked them with the three nearest surrounding stations belonging to the 54 stations relative to 1961-1990. We accepted a station only if every month differs from the corresponding month (average of the 3 nearest stations), in absolute value, less than 10%. In this way, we obtained a new denser dataset made of 158 stations; we rejected 78 stations out of 236.

In figure 163 we show the enlarged 1961-1990 sunshine duration dataset distribution for Italy.

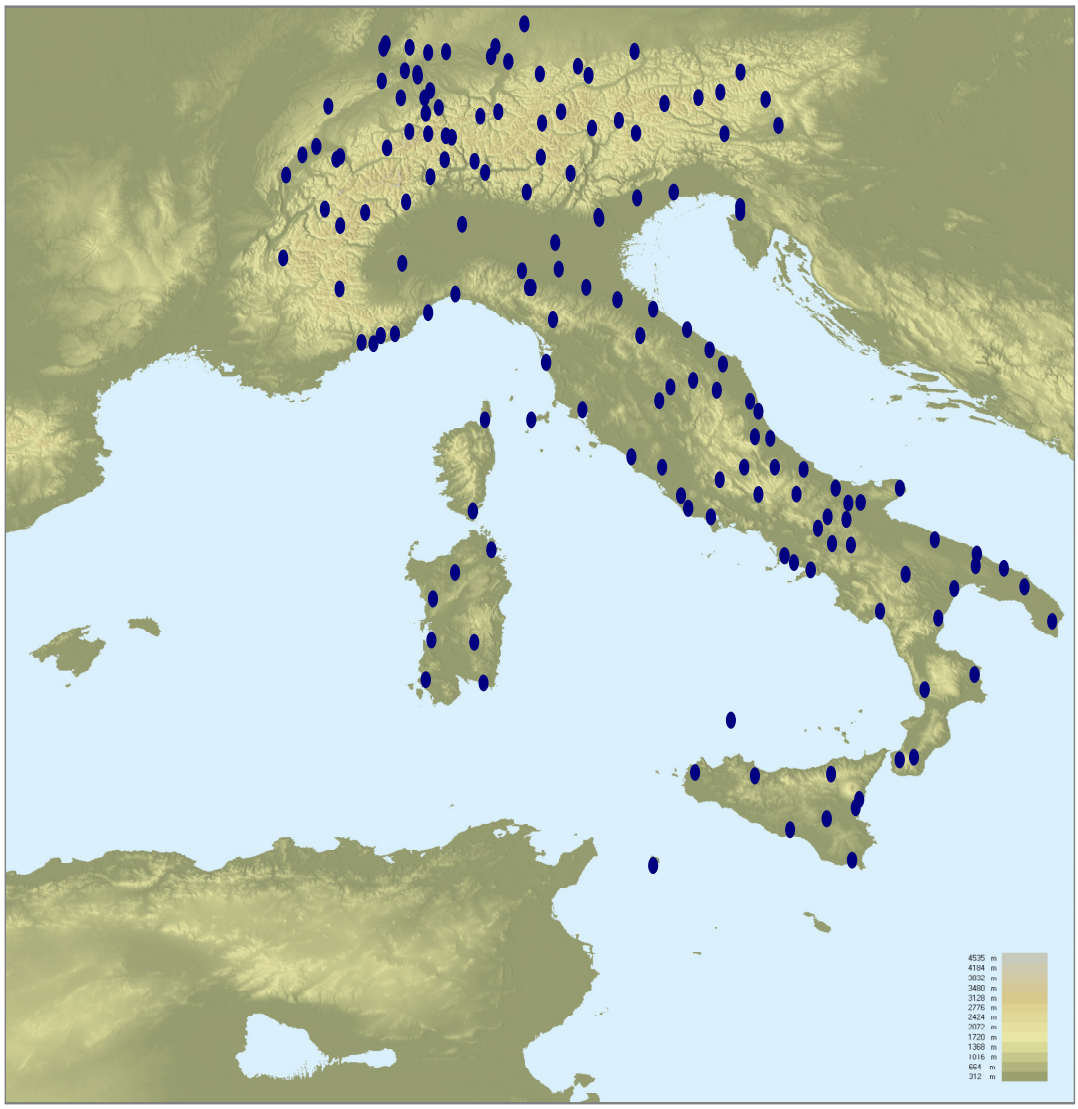

Fig. 163: Sunshine radiation 1961-1990 station distribution for Italy from the enlarged dataset.

6.4.3 From sunshine duration to relative sunshine duration

• The Sun hours ratio

Sunshine duration data are expressed in **hours**, that is, for example, 5.4 h. In order to avoid the latitudinal effects and in order to consider the different astronomical parameters for any month, we need the **relative sunshine duration** that is defined as:

$$R_s = \frac{S}{S_0} \qquad \textbf{(124)}$$

Where S is the number of Sun hours measured by, for example, a Campbell-Stokes sunshine recorder, S_0 is the day length (i.e. the number of hours from sunrise to sunset) and R_S is often called the Sun Hours Ratio.

We used a fundamental hypothesis: the sunshine duration data come from stations located on a flat surface and far from shading obstacles as mountains, hills or walls. This is usually true for stations because the *WMO* recommends placing them under the cited conditions.

• The day length

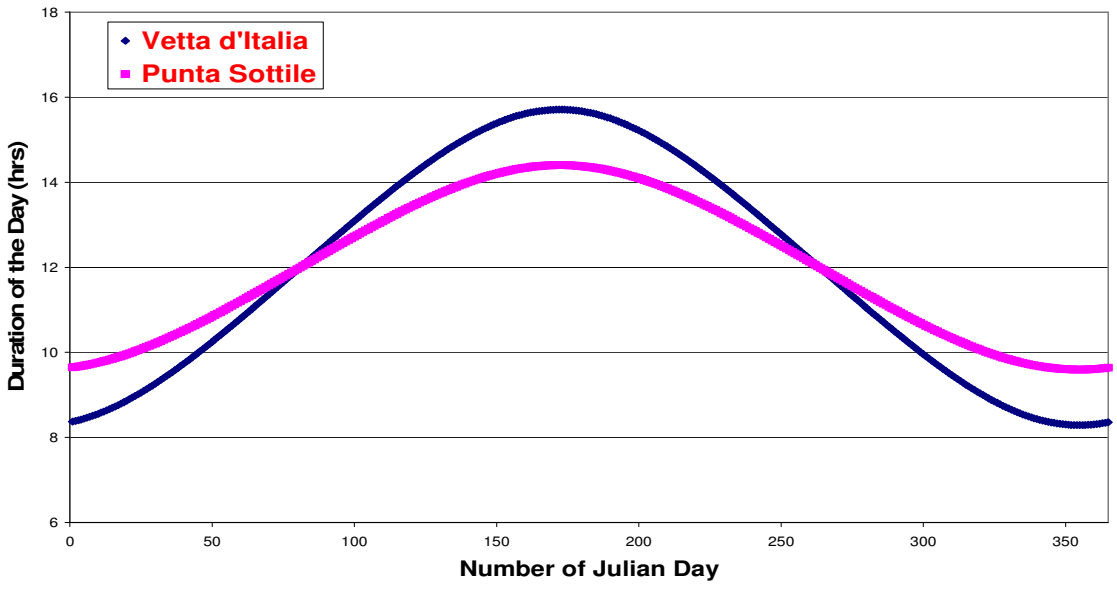

Fig. 164: Number of Sun hours for Vetta d'Italia and Punta Sottile (Lampedusa) vs. number of Julian day

The theoretical duration of the day (see fig. 164, where we show the theoretical duration of the day for Vetta d'Italia and for Punta Sottile during the year), the so-called day length, is the number of Sun hours that a point would receive between sunrise and sunset, if there were no clouds and no shading. It can be used to calculate the Sun Hours Ratio.

Following *Allen et al. (2006)*, the **day length** (**hours**) can be calculated as:

$$S_0 = \frac{2w_{ss}}{15} \qquad \textbf{(125)}$$

Where w_{ss} is the sunset hour angle (see next paragraphs for details).

Let us show the hours of daylight for any latitude and any day of the year.

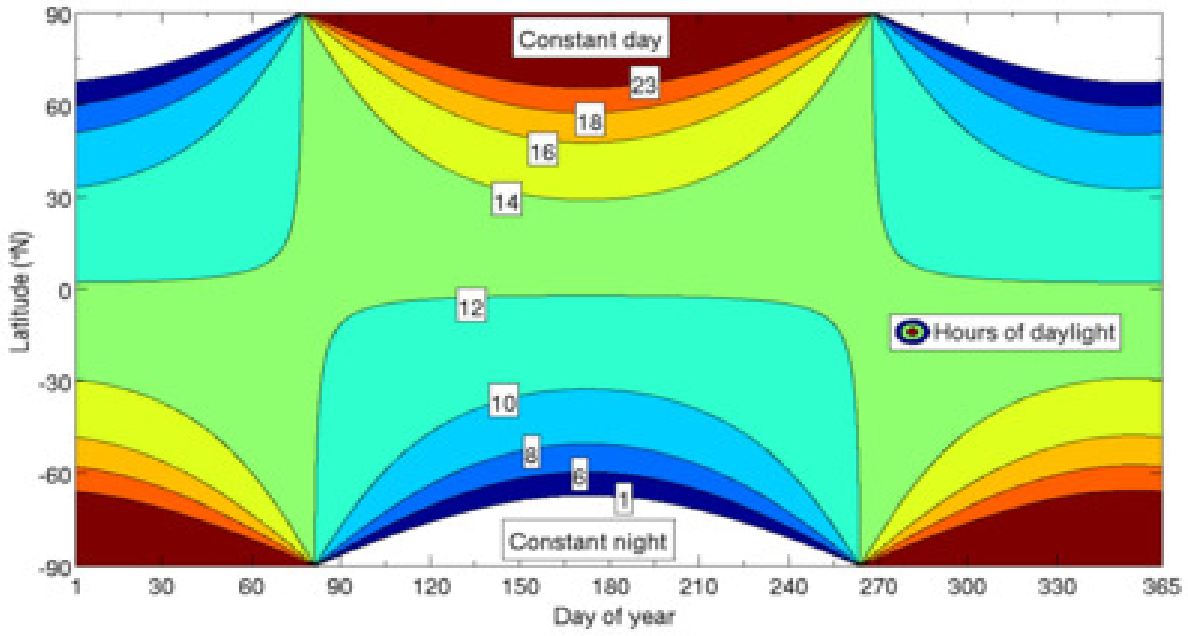

Fig. 165: Number of Sun hours for the globe (Wikipedia, 2010)

The day is longer in winter for lower latitudes in the Northern Hemisphere, while it is longer for higher latitudes in summer. At the equinoxes the theoretical duration is 12 hours everywhere.

• The sunrise angle and the sunset angle

Following *Allen et al. (2006)*, the **sunset hour angle** (w_{ss}) is measured in **degrees** and can be defined as:

$$w_{ss} = \arccos\left(-\tan\phi \tan\delta\right) \quad \textbf{(126)}$$

Where ϕ is the latitude (in radians), δ is the solar declination angle (in radians, see next paragraphs for details).

Equation (126) can be used to derive the time of sunset for any solar declination and latitude in terms of local solar time when sunrise actually occurs.

Similarly, we can define a sunrise equation that quantifies the **sunrise hour angle** (w_{sr}, **degrees**):

$$w_{sr} = -\arccos\left(-\tan\phi\tan\delta\right) \quad \textbf{(127)}$$

The sunset hour angle is positive and the sunrise hour angle is negative because the hour angle is the angular displacement of the sun east or west of the local meridian. This is due to rotation of the Earth on its axis at 15° per hour: morning is negative and afternoon is positive. Of course, the hour angle is null at solar noon. See next paragraph for details on the hour angle equation.

It should be emphasized that in some cases, no sunrise and no sunset occur. In fact, following *Xiaofeng et al. (1996)*, if $(\phi + \delta) < 0°$ no sunrise occurs, whilst if $(-\phi + \delta + 90°) < 0°$ no sunset occurs. Because of the dependence on latitude (ϕ or λ) and solar declination, these values vary not only daily but even from one grid point to another *(Wang et al. 2005)*, although no sunrise or no sunset situations never occur for Italy in flat surfaces, if we exclude shading effects.

The real sunrise takes place when the upper part of the Sun's disk is over the horizon; an observer on the Earth sees the upper border of the Sun's disk with an angle of 0.83° when the Sun's center is on the line of the horizon. Thus the real sunrise takes place approximately 2 minutes earlier than predicted by the above formulas at the Equator, and

the difference increases going to the Poles and at Italy's latitudes; the gap is approximately 5 minutes.

Also, the atmospheric refraction should be taken into account. When we see the Sun over the horizon, its real position is just under the horizon because light is refracted by air. We will deal with refraction corrections later when we describe how to model the solar radiation for sloped surfaces. We did not consider the atmospheric refraction to calculate the day length.

• The hour angle and the equation of time

The hour angle of a point on the Earth's surface is the angle through which the Earth would turn to bring the meridian of the point directly under the Sun. The Earth is rotating, so this angular displacement represents time. In observing the Sun from Earth, the solar hour angle is an expression of time, expressed in angular measurement, most usually degrees, from the solar noon.

According to *Meeus (1998)*, we can define the **solar hour angle** (*h*, **degrees**) as:

$$h = (GMT_{fractionalhour} - 12.00) \cdot 15° + Lon + TC \qquad \textbf{(128)}$$

Where $GMT_{fractional\ hour}$ is the fractional hour expressed in Greenwich Mean Time (e.g., *12:15 GMT* is *12.25* in fractional hour) that can be seen as the Italian Standard Time minus one hour; *Lon* is Longitude (in radians), *TC* is the time correction.

The solar hour angle must be calculated related to *GMT* (Greenwich Mean Time), that is a good approximation of the Universal Time (*UT*) which in turn depends on the sidereal time. In Italy, the clock marks *GMT+1* and we call this time the Italian Standard Time (*IST*) that is the synchronized time for Italy. This is different from the real Local Time (*LT*) that varies from one geographical point to another. Thus, in Italy we have to subtract one hour from the clock time in order to get the universal time.

Time correction can be defined as:

$$TC = 0.004297 + 0.107029 \cdot \cos(g) - 1.837877 \cdot \sin(g) - 0.837378 \cdot \cos(2g) - 2.340475 \cdot \sin(2g) \quad \textbf{(129)}$$

Where g is the fractional year (degrees).

The **fractional year** (**degrees**) can be defined as:

$$g = \frac{360}{365.25} \cdot \left((d_n - 1) + \frac{GMT_{fractionalhour}}{24.00} \right) \quad \textbf{(130)}$$

The time correction is related to the **equation of time**: it is the difference between apparent solar time and mean solar time, both taken at a given place (or at another place with the same geographical longitude) at the same real time *(Burington, 1949)*.

The equation of time varies over the course of a year, in a way that is almost exactly reproduced from one year to the next. Apparent time, and the sundial, can be ahead (fast) by as much as 16 min 33 sec (around 3 November), or behind (slow) by as much as 14 min 6 sec (around 12 February). 4 minutes correspond to 1°.

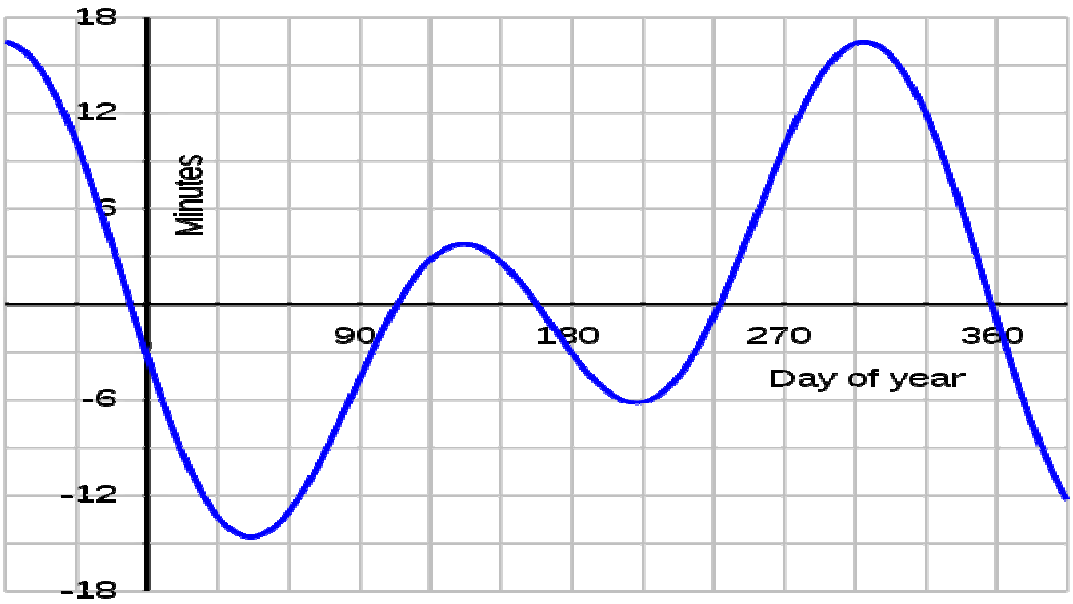

Fig.166: Time-shift (in minutes) during a year from the equation of time.

The equation of time results mainly from two different superposed astronomical causes, each causing a different non-uniformity in the apparent daily motion of the Sun relative to the stars, and contributing a part of the effect: the obliquity of the ecliptic (the plane of the Earth's annual orbital motion around the Sun), which is inclined by about 23.45° relative to the plane of the Earth's equator and the eccentricity and elliptical form of the Earth's orbit around the Sun. The equation of time is also the east or west component of the analemma, a curve representing the angular offset of the Sun from its mean position on the celestial sphere as viewed from Earth. The equation of time was historically used to set clocks.

Let us go back to the hour angle: at solar noon, at the observer's longitude on Earth, the hour angle is 0° with the time before solar noon expressed as negative degrees, and the local time after solar noon expressed as positive degrees. The solar noon can be seen as the moment when the Sun crosses the meridian in "apparent solar time" and the apparent solar time is based on the apparent solar day, which is the interval between two successive returns of the Sun to the local meridian. The solar noon can also be described as the moment when the Sun appears the highest in the sky, compared to its positions during the rest of the day. It occurs when the Sun is transiting the celestial meridian, that is an imaginary great circle on the celestial sphere (it passes through the North point on the horizon, through the celestial pole, up to the zenith, through the South point on the horizon, and through the nadir, and it is perpendicular to the local horizon).

• The solar declination angle

Another important astronomic parameter that must be used to calculate the day length is the **solar declination**. Following *Bristow et al. (1994)* it is expressed in **degrees** (or in radians) and can be defined as:

$$\delta = 23.45 \sin\left(\frac{2\pi}{365}(d_n + 284)\right) \qquad \textbf{(131)}$$

Where d_n is the number of Julian day ($d_n = 1$ for January 1st, $d_n = 365$ for December 31st).

The declination of the Sun (δ) is the angle between the sunrays and the plane of the Earth's Equator, it varies during the seasons and its period is one year. The absolute maximum values ($\delta = 23.45°$) happen at the solstices; the absolute minimum values ($\delta = 0°$) happen at the equinoxes. A more refined expression based on a three order cosine and sine series can be found in literature *(Hartmann, 1994)*, but the solar declination values are approximately the same. The solar declination angle depends only on the Julian day, it does not vary with latitude, thus at Rome, the solar declination angle is the same as Naples in the same day.

In the following picture, we show a graphic representation of the solar declination angle.

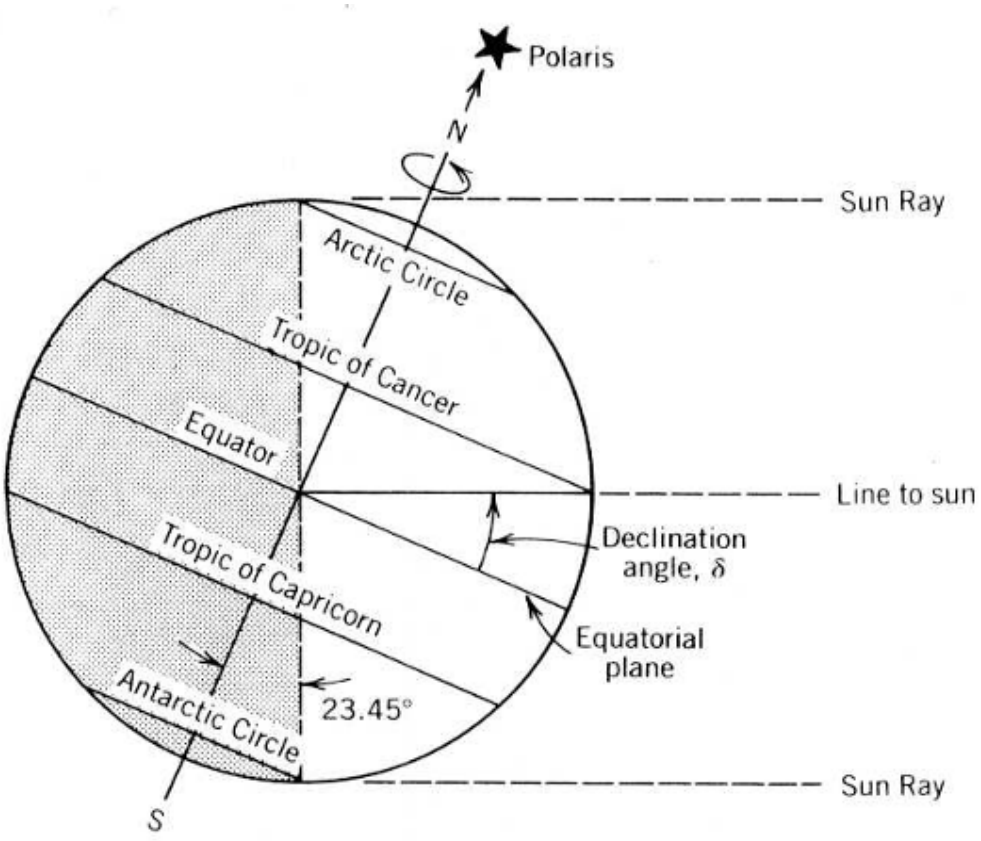

Fig. 167: The solar declination angle (www.powerfromthesun.net)

In the next page, in fig. 167, we show the variation of the solar declination angle during the year

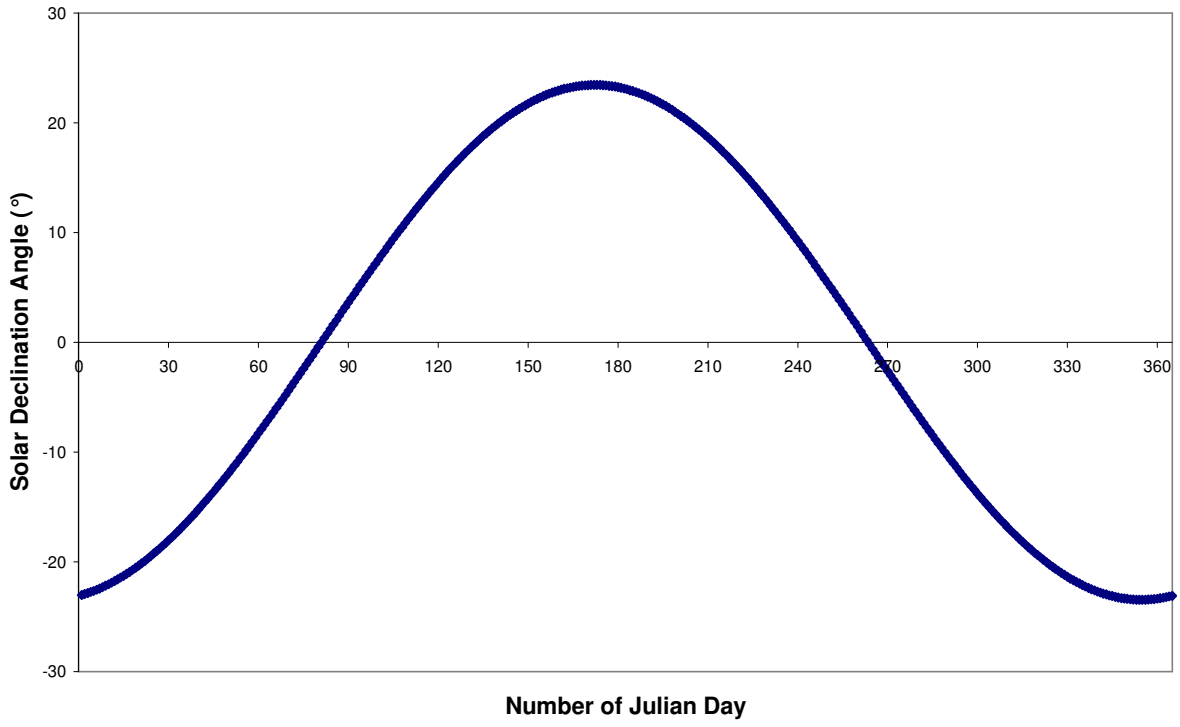

Fig. 168: Daily values of the Solar Declination Angle (in centesimal degrees)

• Calculation of the Sun Hours Ratio: an example

In order to calculate the day length we need to calculate the solar declination. We decided to calculate the average value for each month, not the solar declination for the 15th day of any month as some authors do.

Here there are the average monthly solar declination (in degrees):

(deg)	Jan	Feb	Mar	Apr	May	Jun	Jul	Aug	Sep	Oct	Nov	Dec
Solar Declination	-20.85	-13.33	-2.39	9.49	18.81	23.08	21.10	13.30	1.99	-9.85	-19.05	-23.10

Tab. 38: Average monthly solar declination angle

In the next page we show how we calculate the Sun Hours Ratio for, e.g., the station of Genova Sestri.

Genova Sestri (Longitude: 8.933 °E; Latitude: 44.404 °N; Elevation: 2 m)
Provider: Italian Air Force
Sunshine duration data: 1961-1990 monthly normals

Average sunshine duration for January: 3.4 h

Solar declination for January (see tab. 38) : -20.85°
Sunrise hour angle for January (see equation 127) : -68.10°
Sunset hour angle for January (see equation 126) : 68.10°
Day length for January (see equation 125) : 9.08 h (9 hours and 5 minutes)

Relative sunshine duration for January : 0.374

We calculated the relative sunshine duration for any month for all the 158 stations in our dataset as we did for Genova Sestri.

6.4.4 From relative sunshine duration to the Clearness Index

• The Clearness Index

The basic idea is to correlate the Clearness Index with the solar radiation received by the surface in terms of the Sun Hours Ratio (*Angstrom, 1924).* The Clearness Index is the ratio between the global radiation really received by a surface and the exo-atmospheric radiation received by the same surface on a clear-sky day and it is usually indicated with K_t *(Gueymard, 2001).* The Clearness Index intrinsically provides an estimation of the atmospheric conditions of the sky in the reference period, i.e. the cloudiness and the turbidity of the atmosphere itself. A Clearness Index of 0.5 means that only 50% of the sky is cloudless or free from pollution in the period under investigation. Consequently, only 50% of the exo-atmospheric radiation reaches the surface; in a perfectly clear and non-interacting atmosphere, the clearness index equals 1 and the surface receives the exo-atmospheric radiation as the upper limit of the atmosphere does.

Following *Black et al. (1954)*, the **Clearness Index** (K_t) can be related to relative sunshine duration as:

$$K_t = \frac{H_T}{H_0} = a + b\frac{S}{S_0} \qquad \textbf{(132)}$$

Where H_T is the total global radiation received from the surface, H_0 is the exo-atmospheric radiation, a and b are the coefficients of the linear regression model (see next paragraphs for details).

The Angstrom's formula and its modified versions such as equation (132) should not be used for solar zenith angles smaller than 5° because the refraction effects should not be neglected. The solar zenith angle is the angle between the direction to the Sun and the observer's zenith (straight up direction) *(Antonic, 1998)*, see the next paragraphs for details.

From (133), the **global radiation** (H_T) can be obtained as:

$$H_t = K_t H_0 \qquad \textbf{(133)}$$

Using equations (132) and (133), we can obtain the global radiation values for each station from the sunshine duration data, but the exo-atmospheric radiation (H_0) and the two coefficients a and b must be calculated.

Let us first explain how the exo-atmospheric radiation can be obtained.

• The exo-atmospheric radiation

The exo-atmospheric radiation is the solar incident radiation that reaches the upper limit of the atmosphere and it is equal to the so-called solar constant, multiplied for a correcting quantity, the eccentricity factor, due to the elliptical orbit of the Earth around the Sun. For a real surface on Earth, an angular factor must be introduced: the cosine of the solar angle of incidence, which is the angle between the sunrays and the normal to the ground surface.

The instantaneous **exo-atmospheric radiation** is measured in **W/m²** and, following *Pons et al. (2008)*, for a ground surface on Earth it can be defined as:

$$H_0 = I_0 \cdot E_0 \cdot \cos(\vartheta_{inc}) \quad \textbf{(134)}$$

Where I_0 is the solar constant, E_0 is the eccentricity factor and ϑ_{inc} is the angle between the vector of the sunrays and the normal vector to the surface.

We need a monthly value, that is the daily integrated value for a day that represents the month, in MJ/m² because global radiation data are usually expressed in MJ/m². Consequently, we first need the instantaneous value and then we will integrate between sunrise and sunset. Here we introduce a conversion factor in order to obtain the **instantaneous exo-atmospheric radiation** in **Mj/m²** for a ground surface on Earth. We can write:

$$H_0 = I_0 \cdot E_0 \cdot \cos(\vartheta_{inc}) \cdot \frac{24 \cdot 3600}{2\pi \cdot 10^6} \quad \textbf{(135)}$$

Following *Pons (1996)*, **solar constant** is equal to:

$$I_0 = 1367 \frac{W}{m^2} \quad \textbf{(136)}$$

As it can be found in many papers (*Pons 1996; Pons et al., 200;*), 1,367 W/m² is the value accepted and suggested by *WMO* (World Meteorological Organization) to be considered as constant.

Because of the imperfect elliptical orbit of the Earth, the distance from the Sun (which is in one of the 2 foci of the ellipse) slightly varies during the year, thus it is necessary to introduce the **eccentricity factor**, that can be defined as:

$$E_0 = \left(\frac{d}{d_0}\right)^2 = \sum_{n=0}^{2} a_n \cdot \cos(n \cdot \vartheta_d) + b_n \cdot \sin(n \cdot \vartheta_d) \quad \textbf{(137)}$$

Where d is the distance Sun-Earth, $d_0 = 1.496 \times 10^8\ km$ is the average distance Sun-Earth, θ_d is the "day angle" and the coefficients are $a_0 = 1.00011$, $a_1 = 0.034221$, $a_2 = 0.000719$, $b_0 = 0$, $b_1 = 0.00128$, $b_2 = 0.000077$.

The eccentricity factor is not negligible because it reflects the fact that in January the Earth receives more solar radiation than in July and the difference is about 7%. The eccentricity factor is non-dimensional and it varies between 0.97 (when the Earth-Sun distance is at its minimum) and 1.03 (when the Earth-Sun distance is at its maximum). Some authors prefer to use the value of the eccentricity at the 15th day of each month, some others prefer to use twelve average monthly values (*Wang et al., 2005; Pons et al., 2008; Allen et al., 2006)* and we followed this last convention.

Following *Hartmann (1994)*, the **day angle** can be defined as:

$$\vartheta_d = \frac{2\pi \cdot (d_n - 1)}{365} \qquad \textbf{(138)}$$

Where d_n is the Julian day of the year (see the former paragraphs).

Eventually, if we need the **daily average exo-atmospheric radiation** in **MJ/m²**, we must integrate the cosine of the solar angle of incidence (by choosing the sunrise and the sunset hour angles as limits of integration). We must also use the average monthly solar declination in the calculations (see tab. 38).

$$H_0 = I_0 \cdot E_0 \cdot \int_{sunrise}^{sunset} \left(\cos(\vartheta_{inc})dh\right) \cdot \frac{24 \cdot 3600}{2\pi \cdot 10^6} \qquad \textbf{(139)}$$

Let us show how to calculate the cosine of the solar angle of incidence.

• The cosine of the solar angle of incidence

The angle between the sunrays and the normal to the real surface varies with time because it depends on the solar position in the sky and the cosine of this angle is used to

describe this features *(Kondratyev et al., 1970; Dubayah et al., 1997; Osozawa et al., 2002; Allen et al., 2006*).

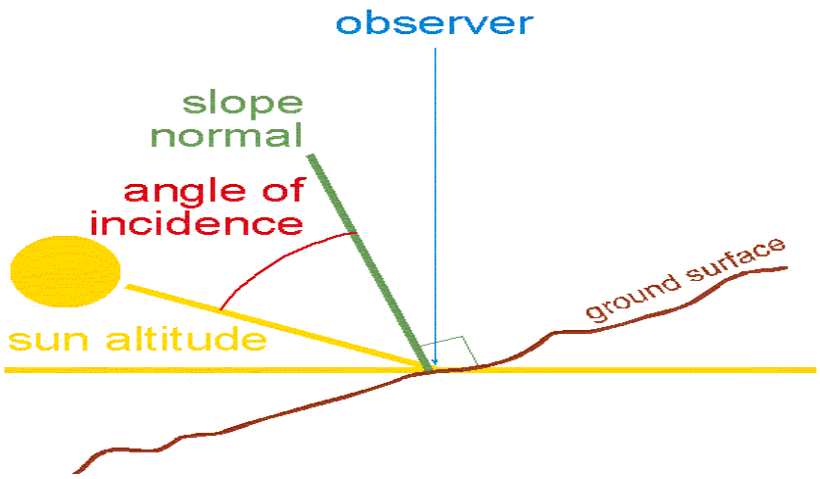

Fig.169: the angle of incidence of the sunrays is the angle between the sunrays and the normal to the surface.

The **cosine of the solar angle of incidence** can be defined as the scalar product between the perpendicular vector to the surface (***n***) and the solar vector (***s***):

$$\cos(\vartheta_{INC}) = \underline{n} \bullet \underline{s} \qquad \textbf{(140)}$$

Where n is the normal vector to the surface and s represents the direction of the sunrays.

Following *Xiaofeng et al., (1996)* and W*ang et al. (2006a)*, the **scalar product between *s* and *n*** can be defined as:

$$\cos(\vartheta_{INC}) = \sin(\delta)\sin(\phi)\cos(s) - \sin(\delta)\cos(\phi)\sin(s)\cos(\alpha) + \cos(\delta)\cos(\phi)\cos(s)\cos(h) +$$
$$+ \cos(\delta)\sin(\phi)\sin(s)\cos(\alpha)\cos(h) + \cos(\delta)\sin(\alpha)\sin(s)\sin(h) \qquad \textbf{(141)}$$

Where δ is the solar declination angle, ϕ is the latitude (in radians), s is the slope of the surface (0° horizontal, 90° vertical), α is the aspect of the surface (0° South, 90° West, -90° East; 180° North), h is the hour angle (0° solar noon, < 0° morning, > 0° afternoon).

In some *GIS* tools (e.g., *Solar Analyst 1.0*) an equivalent formula based on the solar zenith angle is used, instead of the latitude and the solar declination (*Xiaofeng et al., 1996; Dubayah et al., 1997; Antonic, 1998).*

In order to obtain the average monthly global radiation, we need to integrate the cosine of the solar angle of incidence. If we use the average monthly solar declination and we set up the sunrise and the sunset hour angles as limits of integration, we obtain the **daily cosine of solar angle of incidence for the "average day of month"**:

Following *Wang et al. (2006a)* , we obtain:

$$\int_{h_1=w_{sr}}^{h_2=w_{ss}} \cos(\vartheta_{INC})dh = [\sin(\delta)\sin(\phi)\cos(s)](h_2 - h_1) - [\sin(\delta)\cos(\phi)\sin(s)\cos(\alpha)](h_2 - h_1) +$$

$$+ [\cos(\delta)\cos(\phi)\cos(s)](\sin(h_2) - \sin(h_1)) + [\cos(\delta)\sin(\phi)\sin(s)\cos(\alpha)](\sin(h_2) - \sin(h_1)) +$$

$$- [\cos(\delta)\sin(\alpha)\sin(s)](\cos(h_2) - \cos(h_1)) \quad \textbf{(142)}$$

Where h_1 is the sunrise hour angle, h_2 is the sunset hour angle. Starting from midnight, the sunrise also corresponds to the time when $\cos\theta_{INC}$ becomes positive from negative, whereas the sunset corresponds to the time when $\cos\theta_{INC}$ becomes negative from positive.

For a horizontal surface, where our sunshine duration station data should be located, the slope angle is null, thus, **the cosine of the solar angle of incidence for a flat surface** is given by:

$$\cos(\vartheta_{INC}) = \sin(\delta)\sin(\phi) + \cos(\delta)\cos(\phi)\cos(h) = \cos(\vartheta_Z) \quad \textbf{(143)}$$

Where ϑ_Z is the solar zenith angle.

For a horizontal surface, the cosine of the solar angle of incidence equals the cosine of the solar zenith angle. In fact, for a horizontal surface, the normal vector **n** to the surface coincides with the zenith line from the observer to the up direction, hence the angle between **n** and **s** is exactly the zenith angle.

Similarly, the **daily cosine of solar angle of incidence for a flat surface for the "average day of month"** can be defined as:

$$\int_{h_1=w_{sr}}^{h_2=w_{ss}} \cos(\vartheta_{INC})dh = [\sin(\delta)\sin(\phi)]\cdot(h_2 - h_1) + [\cos(\delta)\cos(\phi)]\cdot(\sin(h_2) - \sin(h_1)) \quad \textbf{(144)}$$

That can be equivalently written as:

$$\int_{h_1=w_{sr}}^{h_2=w_{ss}} \cos(\vartheta_{INC})dh = 2\cdot[\sin(\delta)\sin(\phi)]\cdot w_{ss} + [\cos(\delta)\cos(\phi)]\cdot(\sin(w_{ss}) - \sin(-w_{ss})) \quad \textbf{(145)}$$

Where we can use the sunset and sunrise hour angles calculated as in equations (126)-(127).

• Other solar angles: zenith angle, elevation angle and azimuth angle

The solar zenith angle is the angle between the direction to the Sun and the observer's zenith (straight up direction); the solar zenith angle (Z or ϑ_Z, see fig. 170) is the complementary angle to the solar elevation angle (E or γ_S, see fig. 170), thus the cosine of the solar zenith angle is equal to the sine of the solar elevation angle. This quantity does not account for the slope and the aspect because the solar elevation angle is the angle between the direction of the sunrays and the idealized horizon. It varies spatially because of the latitude term and temporally because of the solar declination and the hour angle terms (*Xiaofeng et al., 1996; Antonic, 1998; Corripio, 2003; Pierce et al., 2005)*.

The **solar elevation angle** is given by:

$$\gamma_S = \arcsin(\cos(h)\cdot\cos(\delta)\cdot\cos(\phi) + \sin(\delta)\cdot\sin(\phi)) \quad \textbf{(146)}$$

And the **solar zenith angle** is given by the complementary of the solar elevation angle:

$$\vartheta_Z = \arccos(\cos(h)\cdot\cos(\delta)\cdot\cos(\phi) + \sin(\delta)\cdot\sin(\phi)) \quad \textbf{(147)}$$

The solar azimuth angle (A or ϑ_A, see fig. 170) is defined as the angle between the line from the observer to the Sun projected on the ground and the line from the observer due south. Generally, positive azimuth angles indicate the Sun is east of south, and negative azimuth angles indicate the Sun is west of south *(Kumar et al., 1997)*.

The **solar azimuth angle** is given by:

$$\vartheta_A = \arccos\left(\frac{\cos(h)\cdot\cos(\delta)\cdot\sin(\phi) - \sin(\delta)\cdot\cos(\phi)}{\cos(\gamma_S)}\right) \qquad \textbf{(148)}$$

The solar zenith angle, the solar elevation angle and the solar azimuth do not depend on the surface's slope and aspect, thus their values for a sloped surface are just the values for the corresponding horizontal surface. In the following picture we show the solar zenith angle (Z), the solar elevation angle (E) and the solar azimuth angle (A).

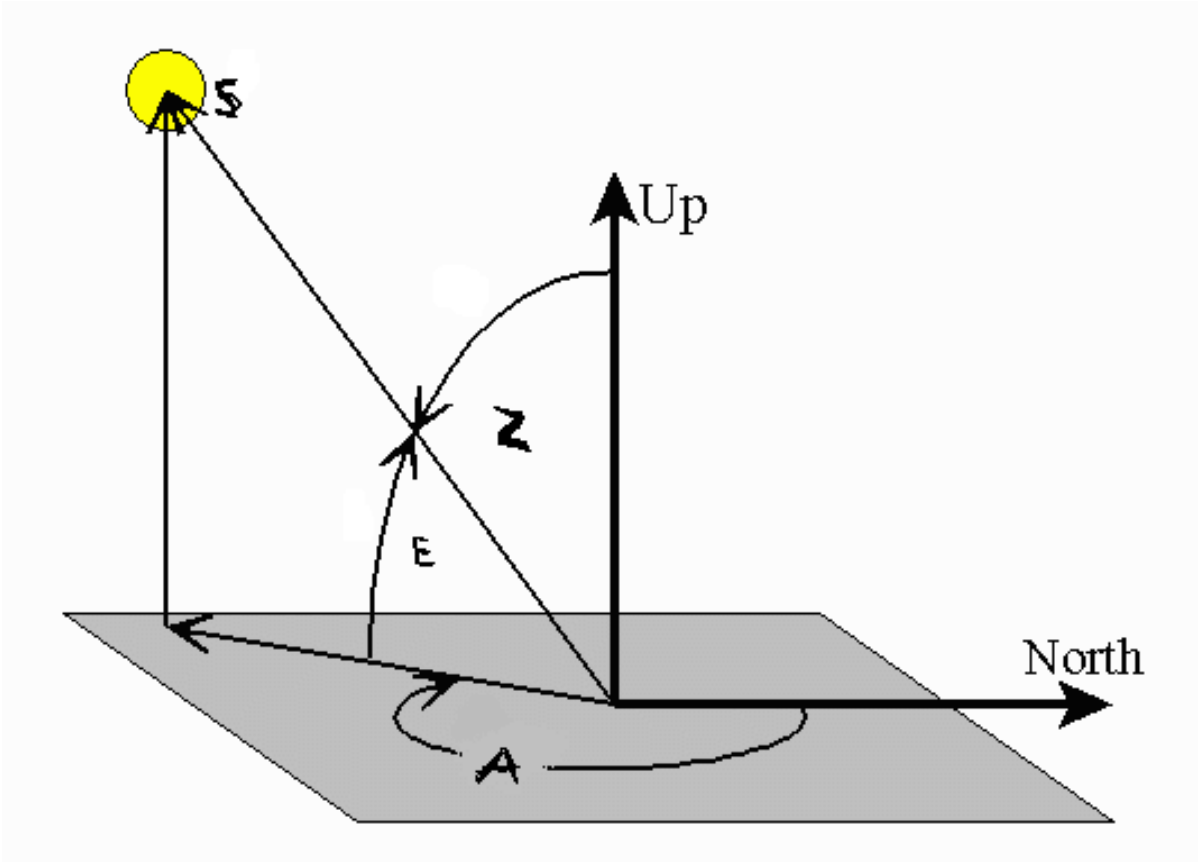

Fig. 170: Z is the solar zenith angle, E is the solar elevation angle, A is the solar azimuth angle

• Calculation of the monthly exo-atmospheric radiation: an example

We calculated the monthly average exo-atmospheric radiation for the stations in our sunshine duration dataset. Here we show an example for January:

Genova Sestri (Longitude: 8.933 °E; Latitude: 44.404 °N; Elevation: 2 m)

Solar declination for January (see tab. 38) : -20.85°
Sunrise hour angle for January (see equation 127) : -68.10°
Sunrise hour angle for January (see equation 126) : 68.10°
Daily integral of the cosine of the solar angle of incidence for January : 0.647
Solar constant : 1,367 W/m^2
Eccentricity factor for January: 1.031

According to equation (139), the exo-atmospheric radiation for January is: 12.544 MJ/m^2

6.4.5 Regression models for the Clearness Index vs. the Sun Hours Ratio

In order to obtain the Clearness Index as in equation (132), the *a* and *b* coefficients of the regression must be calculated. We used two different approaches: the first one deals with calculating the coefficients from sunshine duration data and global radiation data, the second one deals with borrowing the coefficients from similar studies found in literature. We chose the best method by means of checking which approach best reproduces the data, making use of statistical techniques and statistical parameters (*MAE*).

+ Calculation of the *a* and *b* coefficients from sunshine duration and global radiation data for Italy

During the data search, we found, mainly from the Air Force dataset on the Air Force website, 33 stations with both sunshine duration and global radiation monthly normals related to the same period. We calculated the day length (S_0) and the exo-atmospheric radiation (H_0) for each station and we studied the Clearness Indexes versus the relative sunshine durations of the 33 stations by means of 12 different monthly *LR* models.

We found these coefficients:

	a	b	R^2 (%)
Jan	0.163	0.688	82
Feb	0.165	0.706	73
Mar	0.205	0.650	78
Apr	0.179	0.715	82
May	0.183	0.687	88
Jun	0.181	0.677	88
Jul	0.206	0.609	84
Aug	0.222	0.577	84
Sep	0.266	0.521	82
Oct	0.215	0.602	89
Nov	0.184	0.648	90
Dec	0.165	0.666	80
Year	0.181	0.688	89

Tab. 39: Monthly a, b coefficients in K_T vs. R_S regressions

The linear regression models provide good fits especially in summer and autumn (more than 80% of variance explained).

For example in January, the Clearness Index for Italy can be determined as:

$$K_t = 0.163 + 0.688 \frac{S}{S_0} \quad \textbf{(149)}$$

Thus, in January, if the relative sunshine duration is equal to *1,* the Clearness Index is equal to 0.85 (even if a sunshine recorder records sunrays, the sky could be partly overcast or some radiation does not reach the ground surface, thus the $a + b$ sum should not equal 1). Whilst if the relative sunshine duration is null (fully overcast day), the Clearness Index is equal to 0.18 and this value is related to diffuse radiation.

In July, the clearness index for Italy can be determined as:

$$K_t = 0.206 + 0.609 \frac{S}{S_0} \quad \textbf{(150)}$$

Thus, in July, if the relative sunshine duration is equal to 1, the Clearness Index is equal to 0.81, whilst if the relative sunshine duration is null, the Clearness Index is equal to 0.21.

• Borrowing the *a* and *b* coefficients from scientific literature

In scientific literature, many papers dealing with the Angstrom-Black's formula (see equation (132)) can be found, here we list the 8 models we used with our sunshine duration data.

- ***Andretta et. al (1982)*** used a database of 98 sunshine duration records (see also *AMI, 1970* and *Guerrini, 1977*) and found, for Italy:

$$K_t = 0.23 + 0.37\frac{S}{S_0} \qquad \textbf{(151)}$$

This model considers only a single regression valid for every month and, even if it is commonly used in most cases, it should be underlined that the two numeric coefficients vary monthly and in some cases even between two different regions in the same country *(Roderick, 1999)*.

- ***Rietveld (1978)*** used a worldwide dataset and obtained:

$$K_t = 0.18 + 0.62\frac{S}{S_0} \qquad \textbf{(152)}$$

This model provides good estimations if S/S_0 are smaller than 0.4.

- ***Iqbal (1983)*** cited the so called Glover's model and obtained:

$$K_t = 0.29\cos\phi + 0.52\frac{S}{S_0} \qquad \textbf{(153)}$$

This model is valid for latitudes (ϕ) lower than 60°.

- ***Gopinathan et al. (1985)*** used a global dataset and obtained:

$$a = -0.309 + 0.539\cos\phi - 0.0693H + 0.29\frac{S}{S_0}$$
$$b = 1.527 - 1.027\cos\phi + 0.0926H - 0.359\frac{S}{S_0} \qquad \textbf{(154)-(155)}$$

where he also used latitude (ϕ) and elevation (H, in km) as independent variables.

At Italy's latitude (e.g., 42 °N), at sea level (0 m), for a S/S_0 of 0.5, the a coefficient is equal to 0.23 and the b coefficient is equal to 0.59. At the same conditions, if the elevation is 1,500 m, the a coefficient is equal to 0.13 and the b coefficient is equal to 0.46.

- ***Newland (1989)*** obtained:

$$K_t = 0.34 + 0.4\frac{S}{S_0} + 0.17\ln\frac{S}{S_0} \qquad \textbf{(156)}$$

Where the logarithmic model provides good fits for $S/S_0 < 0.2$ and for $S/S_0 > 0.6$.

- ***Akinoglu et al. (1990)*** used a worldwide dataset and obtained:

$$K_t = 0.145 + 0.845\frac{S}{S_0} - 0.28\left(\frac{S}{S_0}\right)^2 \qquad \textbf{(157)}$$

- ***Coppolino et al. (1994)*** used an Italian dataset and obtained:

$$K_t = 0.67\left(\frac{S}{S_0}\right)^{0.45} sen^{0.05}(E) \qquad \textbf{(158)}$$

Where E is the solar elevation angle.

- ***Landsberg et al.*** ***(1997)*** used an Australian and Antarctic dataset and obtained:

$$K_t = 0.23 + 0.5\frac{S}{S_0} \qquad \textbf{(159)}$$

They compared this model with worldwide data and they concluded that equation (159) can be used not only for Australian data but also even worldwide.

In literature, other approaches can be found, for example those that include atmospheric transmission parameters (*Revfeim, 1981)* or that define site-independent coefficients *(McArthur et al., 1981)*, but the most used models are based on regression equations.

On the other hand, *Suhercke (2000)* revised the Angstrom's formula (equation (132)) and theoretically hypothesized that a non-linear correlation between the Clearness Index and the Sun Hours Ratio should be preferred, but this hypothesis is seldom accepted.

A good statistical comparison between some of the cited models and others not reported in this paragraph, by using station data from 77 European stations, can be found in *Soler (1990)*.

• Calculation of the Clearness Index using the a and b coefficients from different approaches

We applied the 8 models found in literature (and applicable to our data) and our model to the 33 station of the *AMI* that report real measured sunshine duration and real measured global radiation data. We calculated the modelled Clearness Indexes data by means of the real measured sunshine duration data and by means of the 9 different *a* and *b* coefficients found in literature and described in the former paragraph. Then we calculated the *MAE* between the modelled Clearness Indexes and the Clearness Indexes as calculated by using real measured sunshine duration data and real measured global radiation data.

Let us remember that our model provides 12 monthly sets of coefficients, whilst the models found in literature provide only one set coefficients for each month.

Thus, we calculated the *MAE* as:

$$MAE = \left| K_T^{modeled} - K_T^{measured} \right| \qquad \textbf{(160)}$$

Where the modeled Clearness Indexes were calculated, e.g., as in equation (159) and the "measured" Clearness Indexes were calculated as the ratio between H_T (measured global radiation data) and H_0 (calculated as in 149) for each of 33 stations.

Here we show the monthly *MAE* obtained by using the different models.

MAE on Kt	Jan	Feb	Mar	Apr	May	Jun	Jul	Aug	Sep	Oct	Nov	Dec	Year
J.Spinoni	0.022	0.024	0.023	0.023	0.022	0.022	0.021	0.020	0.019	0.015	0.017	0.022	**0.021**
Rietveld	0.025	0.034	0.046	0.053	0.045	0.042	0.027	0.024	0.033	0.030	0.024	0.022	**0.034**
Andretta	0.062	0.086	0.107	0.124	0.129	0.136	0.141	0.134	0.131	0.113	0.077	0.055	**0.108**
Glover	0.026	0.044	0.196	0.027	0.028	0.027	0.028	0.033	0.026	0.032	0.051	0.067	**0.049**
Gopinathan	0.028	0.026	0.024	0.026	0.023	0.023	0.025	0.030	0.023	0.019	0.024	0.030	**0.025**
Newland	0.104	0.107	0.122	0.124	0.111	0.102	0.080	0.076	0.092	0.096	0.103	0.100	**0.101**
Akinoglu	0.022	0.028	0.038	0.046	0.043	0.044	0.037	0.031	0.034	0.027	0.019	0.023	**0.033**
Coppolino	0.023	0.030	0.045	0.063	0.070	0.080	0.082	0.069	0.060	0.041	0.023	0.026	**0.051**
Landsberg	0.026	0.036	0.050	0.062	0.059	0.060	0.053	0.048	0.053	0.044	0.027	0.024	**0.045**

Tab. 40: Monthly MAE parameters for K_T calculations

As we can see in tab. 40, our model provides the best results along with Gopinathan's model. Rietveld's model and Akinoglu's model provide small *MAE*, but in spring they are quite high. Coppolino's model and Landsberg's model provide medium *MAE*, while Andretta's model and Newland's model provide the worst results if applied to our data.

Because our model is based on monthly coefficients and because our model provides results comparable with Gopinathan's model (that is by far the most used in literature), even if we based our estimations only on 33 stations, we finally decided to apply our model to all the 158 stations in the sunshine duration dataset and we calculated the monthly Clearness Indexes for each station.

In the end, we multiplied the monthly Clearness Indexes by the monthly exo-atmospheric radiation values as in equation (134) and we obtained the monthly global radiation values in MJ/m^2 for each of 158 stations in our dataset.

In the next paragraph we show an example of such calculations.

+ Calculation of the monthly global radiation for a station: an example

Let us calculate the global radiation for an example station for January.

Genova Sestri (Longitude: 8.933 °E; Latitude: 44.40 4°N; Elevation: 2 m)

Average sunshine duration for January: 3.4 h
Day length for January: 9.08 h
Relative sunshine duration for January : 0.374

Average exo-atmospheric radiation for January: 12.54 MJ/m^2

Clearness Index for January (Spinoni's model): 0.451
(Clearness index for January (Gopinathan's model): 0.471)
(Relative difference between the two models: approximately 4%)

Average global daily radiation for January: 5.66 MJ/m^2

6.4.6 Decomposition models: global radiation split up into direct and diffuse components

• From Clearness Index to diffuse radiation and direct radiation indexes

The main problem to overcome in the creation of a solar model is probably the determination of the diffuse fraction of the radiation received by a surface because of the lack of diffuse radiation in situ measurements. Even where global radiation data were

available, we seldom found papers dealing with data on the beam and the diffuse components *(Gopinathan et al., 1995; De Miguel et al., 2001; Wong et al., 2001)*. This separation can be obtained by means of the decomposition models *(Iqbal, 1983; Spitters et al. 1986*). In such models, from the Clearness Index and/or the sunshine duration data, we can derive the diffuse and direct radiation fractions. In some cases, a solar altitude correction may be added (*De Miguel et al., 2001)*.

For more details on the dependence of the diffuse fraction on atmospheric components, see Chapter 6.3.3.

The **diffuse radiation fraction of the global radiation** received by a surface (or **diffuse radiation index**) is defined as:

$$K_{dif} = \frac{H_{dif}}{H_T} \quad \textbf{(161)}$$

Where H_{dif} is the diffuse radiation and H_T is the global radiation received by the surface.

The **direct radiation fraction of the global radiation** received by a surface (or **direct radiation index**) is defined as:

$$K_{dir} = \frac{H_{dir}}{H_T} \quad \textbf{(162)}$$

Where H_{dir} is the direct radiation and H_T is the global radiation received by the surface.

Dealing with station data, the reflected component of the global radiation can be neglected because stations are usually located over flat surfaces with very low albedo, so the reflected component is usually lower than 1%, and in this case we have:

$$K_{dir} + K_{dif} = 1 \quad \textbf{(163)}$$

The decomposition models are site-dependent models and the coefficients of the regressions are usually valid only for those single regions studied, but in some cases they are applicable worldwide *(Gopinathan, 1988; Gopinathan et al., 1995; Roderick, 1999)*. Nevertheless, it should be reminded that the Northern Hemisphere has a higher diffuse fraction than the Southern Hemisphere. This is because of the higher portion of emerged lands, the higher population density and industrialization that causes higher aerosol and pollutant concentrations which enhance the scattering of the solar radiation *(Roderick, 1999)*.

According to ***Page (1964)***, the diffuse radiation index can be calculated as:

$$K_{dif} = 1 - 1.13K_t \quad \textbf{(164)}$$

According to ***Iqbal (1983)***, the diffuse radiation index can be calculated as:

$$K_{dif} = 0.958 - 0.981K_t \quad \textbf{(165)}$$

According to ***Gopinathan et al. (1985)***, the diffuse radiation index can be calculated as:

$$K_{dif} = 0.878 - 0.3328K_t - 0.53\frac{S}{S_0} \quad \textbf{(166)}$$

Gopinathan et al. (1985) used 40 stations worldwide and compared 5 different models to the measured values, concluding that the best one has to take into account both the Clearness Index and the Sun Hours Ratio. Whilst including latitude would be useless and including the solar angle of declination would not improve significantly the statistical errors.

Roderick (1999) used Australian and Antarctic station data and compared the results obtained with other results valid globally. Roderick's model is divided into three different regressions, according to three intervals for the Clearness Index. In the next page we show the main formula.

$$\begin{cases} K_{dif} = a + bK_t & K_t \le X_0 \\ K_{dif} = c + dK_t & X_0 < K_t \le X_1 \\ K_{dif} = e + fK_t & K_t < X_1 \end{cases} \quad \textbf{(167)}$$

Where X_0 and X_1 are the thresholds for the Clearness Index and *a, b, c, d, e, f* are the coefficients of the three linear regressions.

Usually, the coefficients *a-f* and the limits of the three intervals vary locally, with the exception of the Rodderick's model, that is global-scale verified. We do not report the results because we did not use this model. Similar models can be found in literature, see Chapter 6.3.3 for more details.

Eventually, we decided to use the Gopinathan's model because in literature it is often pointed as the most reliable one and we verified (see the former paragraphs) that the same author created a model for the Clearness Index that fits very satisfactorily to our sunshine duration data.

Therefore we calculated the monthly diffuse fraction (using equation (166)) and consequently the monthly direct fraction of the global radiation (see equation (163)) for the 158 stations of our dataset. Consequently, we obtained monthly direct radiation and diffuse radiation in MJ/m^2 for the 158 stations.

In the next paragraph we show an example of such calculations.

• Calculation of the diffuse component and the direct component fractions of the global radiation: an example

Let us calculate the diffuse and direct radiation fractions for a station for January:

Genova Sestri (Longitude: 8.933 °E; Latitude: 44.404 °N; Elevation: 2 m)

Relative sunshine duration for January : 0.374
Clearness Index for January (Spinoni's model): 0.451

Diffuse fraction for January (Gopinathan's model): 0.506
(Diffuse fraction for January (Page's model): 0.490)
(Diffuse fraction for January (Iqbal's model): 0.516)

Direct fraction for January: 0.494

Diffuse radiation for January: 2.86 MJ/m^2
Direct Radiation for January: 2.80 MJ/m^2

6.4.7 1961-90 direct radiation and diffuse radiation high resolution grids for horizontal surfaces for Italy

For each month, we used the direct and diffuse radiation values corresponding to the 158 stations and we constructed high-resolution grids for Italy by means of an *IDW* spatialization model.

As raster, we used coordinates from the original *USGS GTOPO30 DEM (30-arc-second* horizontal resolution) and as the radial weight we used a Gaussian weight that can be written as:

$$w_i^{rad}(x, y) = e^{-\left(\frac{(d_i(x,y))^2}{c_d}\right)} \qquad \textbf{(168)}$$

Where $d_i(x,y)$ is the distance between a grid cell with a station and the grid cell to be modelled and c_d is the coefficient that regulates the decrease of the weighting factor as:

$$c_d = -\frac{\bar{d}^2}{\ln(0.5)} \qquad \bar{d} = 50km \qquad \textbf{(169)}$$

Where $w^{rad} = 0.5$ when a station is located at 50 km from the grid cell to be modelled, $\bar{d}$ is the radial distance from the grid cell where the weight equals 0.5, i.e., if the station is at 50 km from the grid cell, its weight equals 0.5.

Each grid cell was modelled considering at least 5 stations and the search radius was set up to *250 km*; elsewhere, the grid cell was not modelled. Then, we **smoothed the resulting grids**. We recalculated each grid cell value as the average of the cell itself and the surrounding 8 cells. Such a smoothing was performed in order to avoid discontinuities in areas with a low station density.

It must be underlined that these are **1961-1990 high-resolution grids for horizontal surfaces** because they are based on station data (1961-1990) and calculations related to flat surfaces. Thus we did not use the *DEM* as an elevation raster, but only as a geographic raster.

From now on we will separately discuss the three components of the solar radiation, i.e. the direct, the diffuse and the reflected, for real sloped surfaces. In the end, we will sum up the three components in order to obtain monthly high-resolution grids for global radiation.

6.4.8 1961-90 high-resolution grids for direct radiation on sloped surfaces

From the high-resolution grids for flat surfaces we had to derive high-resolution grids for real sloped surfaces. First, for each month, we used direct radiation grids for horizontal surfaces in order to empirically obtain grids of atmospheric turbidity for Italy. Second, we used a formulation based on a exponential model for the attenuation of the atmosphere, on the turbidity Linke's factor, on the optical properties of the atmosphere, to calculate the direct radiation for a real attenuating atmosphere (see equation (170)). Third, we used the cosine of the solar angle of incidence to evaluate the direct radiation on real sloped surface. Fourth, we implemented an algorithm that considers the shading effect of the surrounding topography for each grid cell.

Eventually, we obtained 1961-1990 high-resolution grids for direct solar radiation component that account for turbidity of the atmosphere, for the real orography and for shading.

• The direct radiation component in an attenuating real atmosphere

According to *Iqbal (1983)*, the **average daily direct radiation component for a sloped surface** in **MJ/m²** is given by:

$$H_{dir} = E_0 I_0 \cdot \frac{24 \cdot 3600}{2\pi \cdot 10^6} \cdot \left(\int_{sunrise}^{sunset} dh \cdot \cos(\vartheta_{inc}) \exp\left[-0.8662 \cdot T_L(m_A) \cdot m_A . \delta_R(m_A)\right] \right) \quad \textbf{(170)}$$

Where T_L is the Linke's turbidity factor, m_A is the optical air mass, δ_R is the Rayleigh's optical thickness (see the next paragraphs for definitions and formulations). $T_L(m_A)$ is often replaced with $T_L(AM2)$ that is the Linke's factor calculated with a fixed value for the optical air mass ($m_A = 2$).

The second part of the formula can be seen as the **total attenuation of the atmosphere**:

$$T = \exp\left[-0.8662 T_L(m_A) \cdot m_A \cdot \delta_R(m_A)\right] \quad \textbf{(171)}$$

Let us describe in details the quantities in equation (170).

• The Rayleigh's optical depth of the atmosphere

The **Rayleigh's optical depth** used in our solar radiation models is the evolution of the Kasten's model *(Kasten et al., 1980)*; many improvements were done to get the model as in *Rigollier et al. (2000) or* in *Jacovides (1997):*

$$\delta_R(m) = \left(6.63 + 1.75m - 0.12m^2 + 0.0065m^3 - 0.00013m^4\right)^{-1} \text{ for } m \le 20 \text{ and } \gamma_S \ge 1.9°$$
$$\delta_R(m) = \left(10.4 + 0.7128m\right)^{-1} \text{ for } m \ge 20 \text{ and } \gamma_S \le 1.9° \quad \textbf{(172)}$$

Where δ_R is the vertical optical thickness of a Rayleigh's atmosphere, that is a clear atmosphere with only permanent gases that scatter light and with no aerosols, no water vapor, no clouds; γ_S is the solar elevation angle (in degrees).

The dependence on m^4 is due to the Rayleigh scattering's dependence, on the fourth power of the wavelength of the incoming radiation. The correction for low solar elevation angles is necessary: in fact, when the Sun is low at the horizon, the blue part of the light spectrum is scattered most and only the red part reaches the Earth's surface. Without the dependence on air mass, for low solar angles, the radiation would be totally attenuated and this would provide unrealistic estimations.

• The optical air mass corrected for elevation and pressure

We can define the **approximated optical air mass** as:

$$m_A = \left(\frac{1}{\cos \vartheta_Z} \right) \tag{173}$$

Where ϑ_Z is the solar zenith angle.

The relative optical path of the sunrays increases when the solar elevation angle decreases, thus the optical air mass should be corrected for elevation, for the refraction of the solar radiation and for pressure *(Kasten et al., 1989)*; thus the formulation shown in equation (173) is too simplistic because it depends only on the solar zenith angle.

Muneer et al. (2000) created a model based on hourly values of a clear sky and an overcast sky radiation that depends on the solar elevation, on the turbidity Linke's factor and on the optical density of the atmosphere. This method is similar to the one used by *Ineichen et al. (2002)*, where an optical mass formulation is used:

$$m = \frac{1}{\sin \gamma_S + 0.50572 \left(\gamma_S + 6.07995 \right)^{-1.6364}} \tag{174}$$

where γ_S is the solar elevation angle (in degrees).

However, this approximation is not valid when the solar elevation is very low and it does not account for the different air pressure at different elevations. The atmospheric refraction takes place when the sunrays go through the atmospheric layers with different

densities that cause the sunrays to be deflected. This effect is not negligible for low solar elevation angles.

The air mass also can be corrected taking into account pressure:

$$m = \frac{p}{p_0} m_0 \qquad \textbf{(175)}$$

Where p_0 is the atmospheric pressure at sea level at standard conditions and equals *1,013.22* mbar.

According to *Kasten et al. (1989),* the air mass can be corrected taking into account the pressure correction and the so-called "paths directions" correction:

$$m = \frac{p}{p_0}\left[\sin(\gamma_S) + 0.15 \cdot (\gamma_S + 3.885°)^{-1.235}\right]^{-1} \qquad for \quad \gamma_S < 20°$$

$$m = \frac{1}{\cos \vartheta_Z} = \frac{1}{\sin \gamma_S} \qquad for \quad \gamma_S > 20° \qquad \textbf{(176)}$$

Where γ_S is the solar elevation angle and ϑ_Z is the solar zenith angle.

The m value for solar elevation angles smaller than 20° is calculated using some approximations, that is an air density of 1.225 Kg/m^3 and a constant refraction index for air (at 700 nm and 0 meters elevation). The m value at the horizon is still not good because it is underestimated, thus, according to *Kasten et al. (1989)* it can be recalculated using the "apparent elevation" as:

$$m = \frac{p}{p_0}\left[\sin(\gamma_S^{\,ref}) + 0.5057 \cdot (\gamma_S^{\,ref} + 6.07995°)^{-1.6364}\right]^{-1} \qquad \textbf{(177)}$$

Where γ_S^{ref} is the solar elevation angle corrected for the apparent elevation.

The apparent elevation angle is defined as the elevation corrected by the refraction and is computed according to *Rigollier et al. (2000)*:

$$\gamma^{ref} = \gamma_S + \Delta\gamma_{ref} \quad \textbf{(178)}$$

Where:

$$\Delta\gamma_{ref} = 0.06136 \cdot \left(\frac{180}{\pi}\right) \cdot \left(\frac{0.1594 + 1.123 \cdot \left(\frac{180}{\pi}\right) \cdot \gamma_S + 0.06566 \cdot \left(\frac{180}{\pi}\right)^2 \cdot {\gamma_S}^2}{1 + 28.9344 \left(\frac{\pi}{180}\right) \cdot \gamma_S + 277.397 \cdot \left(\frac{\pi}{180}\right)^2 \cdot {\gamma_S}^2} \right) \quad \textbf{(179)}$$

The pressure can be corrected with the elevation correction as in *Geiger et al. (2002)*:

$$\frac{p}{p_0} = e^{-\left(\frac{Elevation}{8434,5}\right)} \quad \textbf{(180)}$$

Where 8,434.5 m is the scale height of the Rayleigh's atmosphere near the Earth's surface.

With the refraction correction for solar elevation angle and the elevation correction for pressure, the optical air mass has its best formulation.

• The turbidity Linke's factor and the Angstrom's coefficient

The atmospheric transmission can be described with the help of the Linke's turbidity factor. The Linke's factor depends especially on the air mass, the water vapor, the gases and the aerosols *(Rigollier et al., 2000)* and represents the number of clean dry atmosphere necessary to produce the same attenuation of the real atmosphere. The average value for Europe is 3.5, but it varies locally; the attenuation increases with T_L because a higher turbidity means higher scattering and absorption processes. T_L depends on the air mass (indicated with m) that is not available everywhere, hence this problem is often moved around imposing a constant value of $m = 2$ for calculating T_L *(Kasten et al., 1989)* or it is

derived inversely from beam pyrheliometric measurements *(Ineichen et al., 2002; Jacovides, 1997)* or local data *(Kasten et al., 1984, Dogniaux, 1976)*.

The Linke's factor can also be seen as the ratio between the total optical depth and the Rayleigh's optical depth. $T_L = 0$ means a non-attenuating atmosphere, $T_L = 1$ means a pure Rayleigh's atmosphere with no aerosols and only molecular scattering, $T_L = 3\text{-}4$ means a quite turbid and non-windy atmosphere, $T_L = 6$ means a very dirty and polluted atmosphere.

The Linke's turbidity factor is also used in *GIS* tools as *r.sun* and in the European Solar Radiation Atlas (*ESRA: Beyer et al., 1997; Rigollier et al., 2000; Page et al., 2001)*.

A similar turbidity's coefficient is the Angstrom's coefficient that quantifies the effects of the aerosols and varies from 0 (very clear atmosphere) to 0.4 (very dirty atmosphere) (see *Jacovides (1997)* for more details).

The combined use of the Linke's factor and Angstrom's coefficient accounts for the attenuation of the direct and the diffuse radiation in a real atmosphere and for the diffraction and the refraction effects *(Beyer et al., 1997)*. The Angstrom's coefficient is rarely used as an independent quantity in literature (*Jacovides, 1997*), but it is often used to obtain a Linke's turbidity modified factor that accounts best for the aerosol extinction and depends even on the Angstrom's coefficient (e.g., *Valko, 1961)*. Other authors (*Jacovides, 1997*) calculate the Angstrom's coefficient from the Linke's factor obtained from pyrheliometric measurements and they divide the atmosphere in rather dry, medium humid and very wet conditions, depending on the water vapor content.

• Empirical derivation of monthly Linke's factor grids from 1961-1990 high-resolution monthly direct radiation grids for flat surfaces

First, we made some assumptions: the turbidity Linke's factor has a high spatial coherence, thus a Linke's factor low-resolution grid (one value for each 0.5° x 0.5° grid cell) would be enough. Furthermore, the Linke's factor describes the turbidity of the atmosphere and it is not linked to the ground orography. Thus we can calculate the Linke's factors using the direct radiation for horizontal surfaces and then we can use the same values when we calculate the direct radiation for real sloped surfaces.

In order to create high-resolution grids for real sloped surfaces, we first needed the turbidity Linke's factor for Italy and we derived it empirically from the **daily direct radiation for a flat surface for the "average day of month"** (in **Mj/m²**), where we used the average monthly value of solar declination angle:

$$H_{dir} = E_0 I_0 \cdot \frac{24 \cdot 3600}{2\pi \cdot 10^6} \cdot \left(\int_{sunrise}^{sunset} dh \cdot \cos(\vartheta_Z) \exp\left[-0.8662 \cdot T_L(m_A) \cdot m_A . \delta_R(m_A) \right] \right) \quad \textbf{(181)}$$

Where the cosine of the solar angle of incidence has been replaced by the cosine of the solar zenith angle.

Let us define the conversion factor from W/m² to MJ/m²:

$$\kappa = \frac{24 \cdot 3600}{2\pi \cdot 10^6} \quad \textbf{(182)}$$

In equation (179) we made the following steps: we calculated monthly H_{dir} for flat surfaces for each grid point of the *DEM* and we extracted monthly E_0 and constant I_0 from literature. For any time interval and any point of the grid, we can calculate $\cos\vartheta_Z$ by equation (143), m_A by equations (173)-(180), $\delta_R(m_A)$ by equation (172); k is a constant.

In order to create a low-resolution (0.5° x 0.5°) grid for the Linke's factor, we first selected 193 grid points which represent Italy as in fig. 171. For each point and for every month, we used the corresponding direct radiation in Mj/m² for a flat surface, the corresponding astronomic parameters (the day length, the solar declination angle, the solar elevation angle, the solar zenith angle, the eccentricity factor), the corresponding constraints (the solar constant and the conversion k factor) and the corresponding atmospheric parameters (the optical air mass and the Rayleigh's optical density). This was in order to obtain a T_L value for each grid cell and for each month.

Eventually, we would be able to obtain 12 monthly 1961-1990 low-resolution grids for Italy for the Linke's factor.

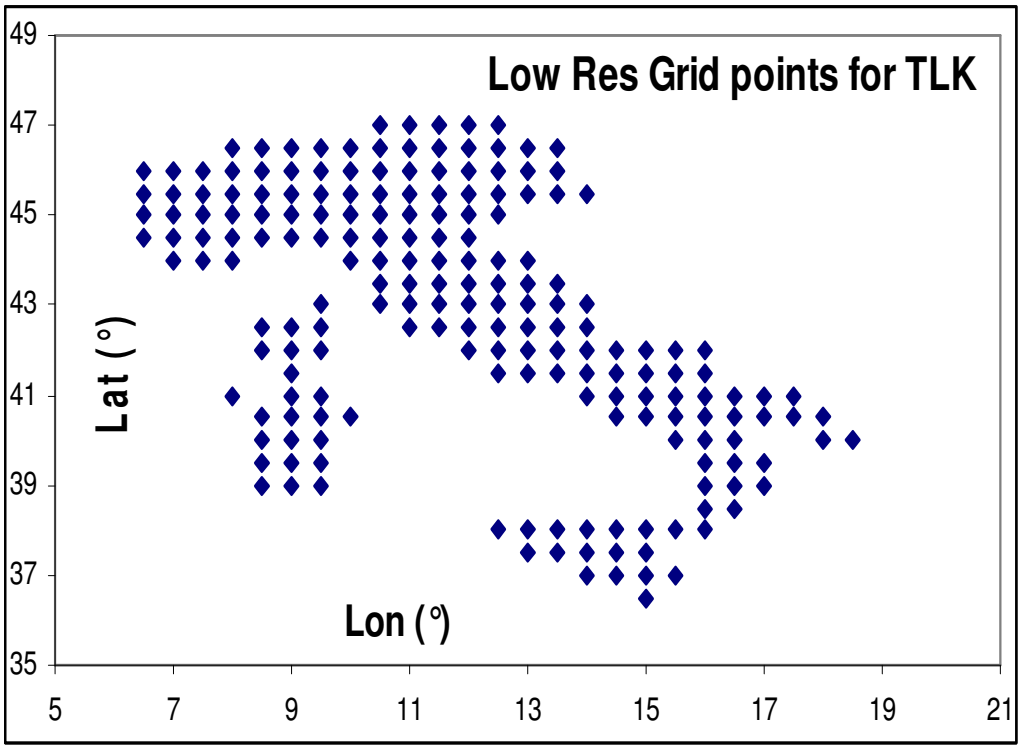

Fig. 171: low-resolution grid points for the turbidity Linke's factor monthly grids.

In order to obtain 12 monthly discrete grids for the Linke's factor we wrote a Fortran code subdivided into many steps. We repeated the same procedure for each grid point (out of 193 grid points) and for every month.

First step: we calculated the sunrise hour angle and the sunset hour angle and we subdivided the "day length" into 100 intervals.

$$Int = \frac{1}{100} \cdot \left| w_{sr} - w_{ss} \right| \qquad \textbf{(183)}$$

Where w_{ss} and w_{sr} must be expressed in radians.

The limits of the first interval are $h_1 = w_{sr}$ and $h_2 = h_1 + Int$, the limits of the second interval are h_2 and $h_3 = h_2 + Int$, …, the limits of the 100th interval are $h_{100} = h_1 + (99 \cdot Int)$ and $h_{101} = w_{ss}$.

Second step: for each interval, we calculated the solar elevation angle (0° for sunrise and sunset, maximum for solar noon) and if it was smaller than 20° we recalculated it introducing the refraction correction.

Third step: for each interval, if the solar elevation angle was smaller than 20°, we used equations (177)-(178)-(179) to calculate the optical air mass m_A, whilst if the solar elevation angle was higher than 20° we used the second equation of equation (176). We did not account for the elevation correction of pressure because our sunshine duration stations were all below 2,000 m, with the exception of Plateau Rosa (approximately 3,400 m)

Fourth step: for each interval, if the optical air mass m_A was higher than 20 (which corresponds to solar elevation angle lower than *1.9°*) we used the first equation in (172) to calculate the Rayleigh's optical density of the atmosphere, whilst if m_A was lower than 20 (which corresponds to solar elevation angle higher than *1.9°*) we used the second equation in (172).

Fifth step: for each interval we calculate the average value of the cosine of the solar angle of incidence (which corresponds to the solar zenith angle for flat surfaces).

Sixth step: we chose the average turbidity Linke's factor for Europe ($T_L = 3.5$) and, for each interval we calculated the direct radiation received from the flat surface by means of the following formula showed, e.g., the 50th interval:

$$\left(H_{dir}(T_L^*)\right)_{i=50} = E_0 I_0 \cdot \kappa \cdot \left(\int_{h_{50}}^{h_{51}} dh \cdot \cos(\vartheta_Z) \exp\left[-T_L^*(m_A) \cdot m_A . \delta_R(m_A) \right] \right) \qquad \textbf{(184)}$$

Where $T_L^* = 0.8662 \cdot T_L$ and where i is referred to the *i-th* interval (out of 100).

Seventh step: we summed up all the direct radiation values of the 100 intervals and we obtained 12 (for each month) temporary direct radiation values for each grid point.

$$H_{dir}(T_L^*) = \sum_{i=1}^{100} \left(H_{dir}(T_L^*)\right)_i \qquad \textbf{(185)}$$

Eighth step: for each grid point and for each month, we compared the direct radiation value obtained by (184) with the direct radiation value obtained from:

$$H_{dir} = H_T \cdot K_{dir} \quad \textbf{(186)}$$

Where we obtained H_T from (133), using the Clearness Index values calculated by equation (132) and *a, b* coefficients as in tab. 39; where we obtained K_{dir} from equation (166).

In other words, we compared the direct radiation values obtained by means of equations and models based on sunshine duration data (see Chapters 6.4.3, 6.4.4, 6.4.5) with the direct radiation values obtained by means of equation (181) of atmospheric attenuation using a Linke's factor of 3.5.

Consequently, we obtained:

$$\Delta_{H_{dir}} = \left| H_{dir} - H_{dir}(T_L^*) \right| \quad \textbf{(187)}$$

Ninth step: the Fortran code replaced the random T_L^* value with a set of discrete values for T_L^* that ranges from 0.100 to 15.000 (the step is 0.001) and estimated the T_L^* that minimizes Δ_{Hdir}. Such a value represents the 1961-1990 turbidity Linke's factor for the considered grid cell and for the considered month.

It is sufficient to repeat such an estimation for all the 193 grid points for all 12 months in order to get low-resolution monthly grids of T_L for Italy in the reference period 1961-1990 (that is the period related to the sunshine duration data used to obtain H_{dir} used in equation (186)).

In the next page we show the low-resolution grids for January and July (1961-1990) for the turbidity Linke's factor. Notice that we used, as many authors do, a T_L value that includes the 0.8662 coefficient. i.e. a T_L^* value in the calculations and in figures 172-173.

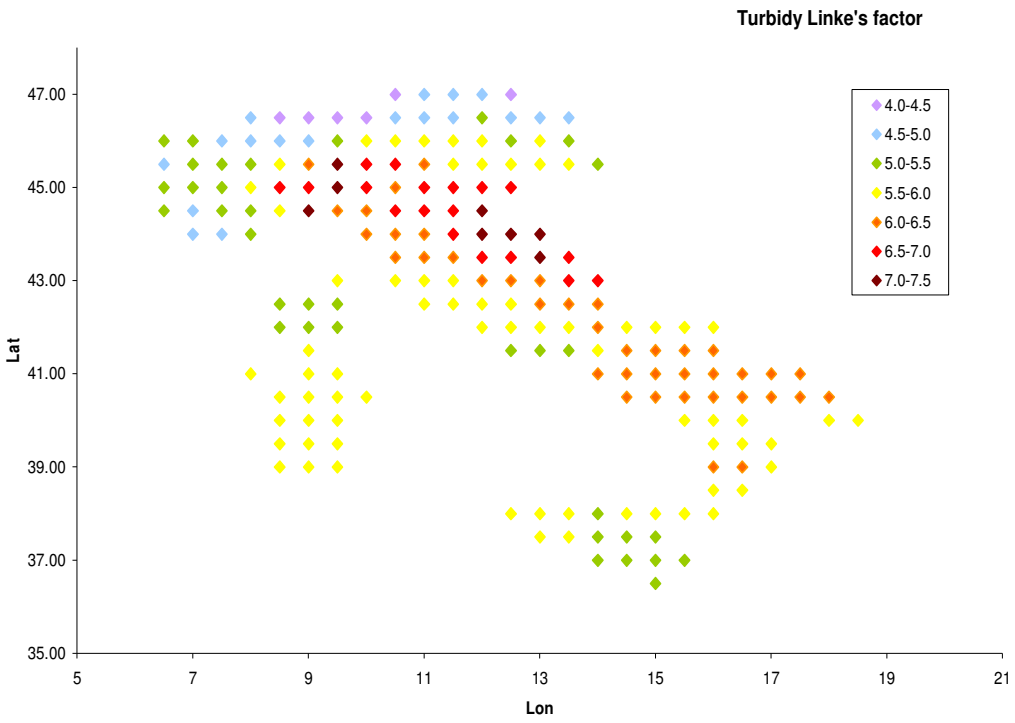

Fig. 172: 1961-90 January grid for the turbidity Linke's factor

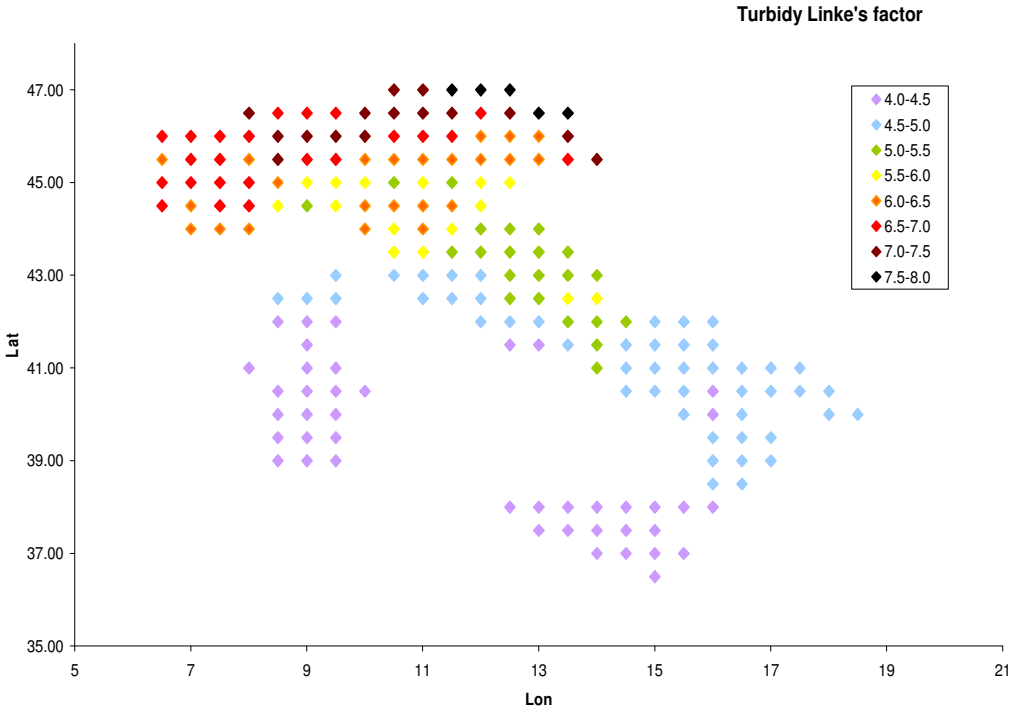

Fig. 173: 1961-1990 July grid for the turbidity Linke's factor

In winter, the turbidity Linke's factor is the highest in the Po Plain due to fog, pollution and clouds. Whilst in summer is the highest over the Alps and is the lowest in the great islands. In fact, precipitations and clouds are more frequent in northern regions than in southern regions in summer.

Tenth step: by means of a *IDW* spatialization model we obtained monthly high-resolution grids from monthly low-resolution grids. We used the Gaussian weight of equation (168) and we set up a distance parameter of 50 km as in equation (169). We did not set a search radius because we had a regularly spaced grid. On the other hand, we considered 9 stations for each grid point in the weighting process.

Eleventh step: we smoothed the 12 monthly high-resolution grids of the Linke's factor with a 3 x 3 cells scheme. We substituted the grid cell value with the average value of the 8 surrounding cells and of the grid cell itself.

Let us set T_L^{ok} for the Linke's factors obtained with this methods

• Direct radiation on a sloped surface: the shading problem

In order to obtain the high-resolution monthly grids for **daily direct radiation on real sloped surfaces** (in **Mj/m²**), we used the *USGS GTOPO30* digital elevation model, from which we calculated, for each grid cell, a slope value and an aspect value. The basic formula is, for a certain grid cell:

$$H_{dir}(T_L^{ok}) = E_0 I_0 \cdot \kappa \cdot \left(\int_{sunrise}^{sunset} dh \cdot \cos(\vartheta_{inc}) \exp\left[T_L^{ok} \cdot m_A . \delta_R(m_A) \right] \right) \qquad \textbf{(188)}$$

Where T_L^{ok} was calculated as discussed in the former paragraph; we replaced ϑ_Z (flat surfaces) with ϑ_{inc} (sloped surfaces). Let us notice that for a sloped surface, the sunset and the sunrise hour angles are the same angles calculated for a corresponding flat surface.

Using the monthly high-resolution grids of the Linke's factor, we can calculate the daily direct radiation for a sloped surface as in equations (183)-(184)-(185), just replacing

ϑ_Z with ϑ_{inc} in equation (181) and using, in this case, the elevation correction for pressure (equation (180)) because of the wide elevation range (0 – 4,810 m) of Italy. However, this procedure is not valid for a real sloped grid cell because a sloped surface does not receive direct radiation from sunrise to sunset. In fact, if a surface is west-facing, due to the fact that the Sun rises in the east, the surface will receive sunrays only after a certain time (that is, when the solar hour angle is higher than a certain value) that depends on the slope inclination, on the slope aspect of the surface, on the solar elevation angle and so on.

A sloped surface could provide negative values of the cosine of the solar angle of incidence and this lead to negative direct radiation fraction that is not realistic; furthermore, this methodology does not account for the topography that surrounds the sloped grid cell and could shade the grid cell.

Let us show how the surrounding topography can shade a grid cell as illustrated in *Zaksek et al., 2005*.

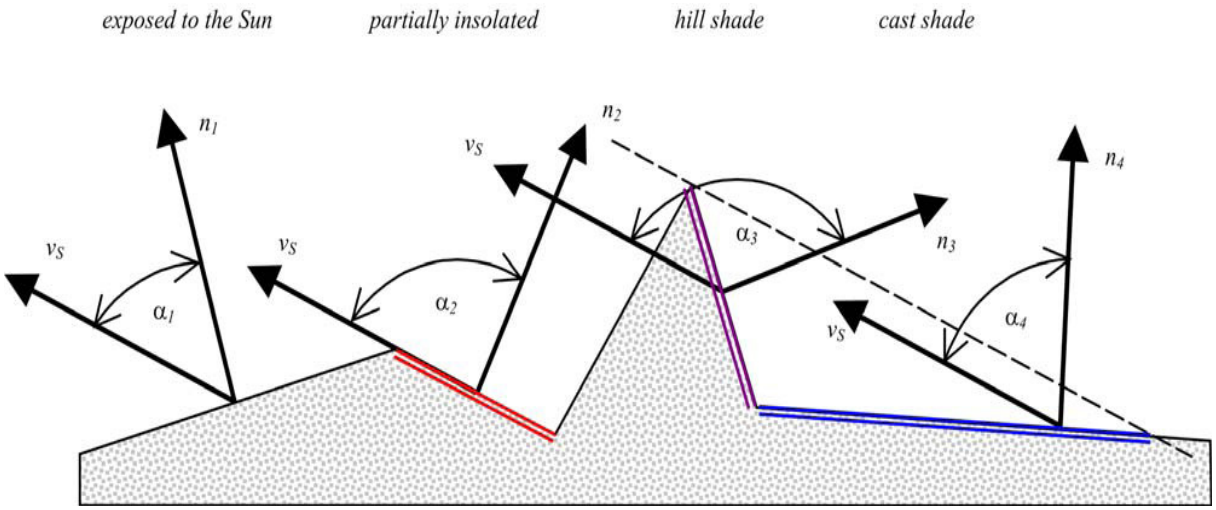

Fig. 174: The angle between the sunrays vector and the normal vector to the ground surface is indicated as α: various angle of incidence correspond to different shading configurations. A) Exposed to the Sun; B) Partially insolated; C) Hill shade; D) Cast shade. (Zaksek et al., 2005)

In fig. 174 the solar angle of incidence is indicated as α, that is: $\vartheta_{inc} = \alpha$.

We can divide into:

A) $\vartheta_{inc} < 90°$ and no shading topography (α_1 ; no shading): the surface receives direct solar radiation ;

B) $\vartheta_{inc} = 90°$ (α_2 ; border situation): the solar radiation is parallel to the surface: the direct radiation is a grazing radiation for the surface (no shading for our code) ;

C) $\vartheta_{inc} > 90°$ (α_3 ; hill-shading): the surface does not receive direct solar radiation but only diffuse and reflected radiation;

D) $\vartheta_{inc} < 90°$ and shading topography (α_4 ; cast shading): the surface does not receive direct solar radiation but only diffuse and reflected radiation .

If situation B occurs, we approximated it as a no shading situation.

We wrote a Fortran code that calculates, for each grid cell, for each month, the "possible" direct solar radiation for each interval and then it sums up the 100 values to get the daily direct solar radiation in Mj/m^2.

In any interval where $cos\vartheta_{inc} < 0$ (hill-shading), the direct radiation received by the grid cell is null, thus the Fortran code sets up $cos\vartheta_{inc} = 0$.

In any interval where $cos\vartheta_{inc} \geq 0$ (no shading or cast shading), the Fortran code calculates if cast-shading occurs or if the grid cell is directly irradiated. In case D, the direct radiation received by the grid cell is null, thus the Fortran code sets up $cos\vartheta_{inc} = 0$, in case A, direct radiation can be calculated.

Let us have a deeper look at how the Fortran code accounts for $cos\vartheta_{inc} \geq 0$:

- First, it selects a surrounding area of 400 km^2 for each grid cell ;
- Second, it calculates the solar azimuth angle for each interval (out of 100) ;
- Third, it searches for the grid cell with the highest elevation on the azimuth direction (see fig. 170).
- Fourth, if the grid cell under investigation is the highest one on the azimuth direction, the grid cell is not cast-shaded, thus the direct solar radiation received can be calculated ;
- Fifth, if the grid cell under investigation is not the highest one, the Fortran code calculates the angle between the grid cell's surface and the straight line from the grid cell to the top of the obstacle. If such an angle is smaller than the solar elevation angle ($z_3 < z_0$ in fig. 175), the grid cell is exposed to the direct radiation. If such angle is higher than the solar elevation angle, the grid cell is in cast shade ($z_1 <$

z_0 in fig. 175); else if such angle equals the solar elevation angle ($z_2 = z_0$ in fig. 175), the grid cell is on the border situation between light and shadow.

-

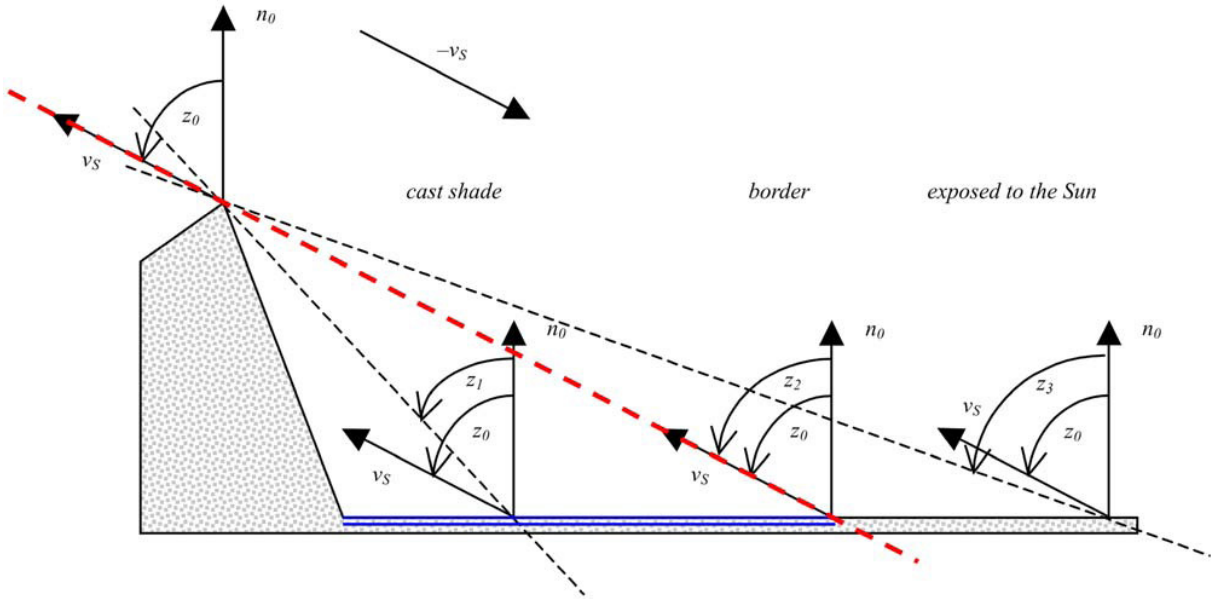

Fig. 175: Representation of the cast shading: the grid cell "behind" the obstacle can be cast-shaded, partially insolated on the border situation or exposed to the Sun (Zaksek et al., 2005). z_0 is the solar elevation angle.

Some authors use pre-packed *GIS* tools, such as *OMBRA*, *INSOLDIA (Pons et al., 2008)*, *HILLSHADE*, *MOD-SHADOWS (Kumar et al., 1997)*, in order to account for shading effects, but these codes are usually too simplistic for high-resolution climatologies.

In the end, for each grid cell and for each month, we have:

$$H_{dir}(T_L^{OK}) = \sum_{i=1}^{100} \left(H_{dir}(T_L^{OK}) \right)_i \qquad \textbf{(189)}$$

where $(H_{dir}(T_L^{OK}))_i = 0$ in any *i-th* interval where hill-shading or cast-shading occurs.

We must underline that a resolution of *30-arc* second is too low to capture in the best way the shading effects of the complex orography in a mountain environment. One or two orders of magnitude higher resolution would probably be better in order to create a very detailed model of the shading effects.